REPUBLIQUE ALGERIENNE DEMOCRATIQUE ET POPULAIRE
MINISTERE DE L'ENSEIGNEMENT SUPERIEUR ET DE LA RECHERCHE SCIENTIFIQUE
UNIVERSITE YAHIA FARES DE MEDEA
FACULTE DE TECHNOLOGIE
DEPARTEMENT DE GENIE MECANIQUE

Cette thèse intitulée :

Etude Numérique de l'Effet De la Forme de la Particule sur son Comportement en Vol et a l'Impact Durant le Processus de la Projection Thermique

EST PRESENTEE EN VUE DE L'OBTENTION
DU DIPLOME DE DOCTORAT EN GENIE MECANIQUE.

Option : Génie des Matériaux.

Par :

BOUKHAZANI Fathi.

Soutenue le : 18/04/2026.

DEVANT LE JURY COMPOSE DE :

Nom et Prénom	Grade	Institution d'affiliation	Désignation
CHIBA Younes	Prof.	Université de Médéa	Président
REBHI Redha	MCA.	Université de Médéa	Directeur de thèse
KEZRANE Mohamed	Prof.	Université de Médéa	Co-directeur de thèse
ELMOHRI Abdennour	MCA.	Université de Médéa	Examinateur
BENSEDIRA Sidali	MCA	Université de Blida	Examinateur

Année Universitaire 2025-2026

PEOPLE'S DEMOCRATIC REPUBLIC OF ALGERIA
MINISTRY OF HIGHER EDUCATION AND SCIENTIFIC RESEARCH
UNIVERSITY YAHIA FARES OF MEDEA
FACULTY OF TECHNOLOGY
DEPARTMENT OF MECHANICAL ENGINEERING



THESIS entitled:

Numerical Study of the Effect of Particle Shape on its in Flight and Impact Behavior During the Thermal Spraying Process

IS SUBMITTED FOR THE PURPOSE OF OBTAINING
PH. D DEGREE IN MECHANICAL ENGINEERING.
option: Materials Engineering.

BY

BOUKHAZANI Fathi.

Presented on 04/18/2026.

IN FRONT OF A JURY COMPOSED OF:

Last and first name	**Grade**	**Institution of affiliation**	**Designation**
CHIBA Younes	Prof.	Université de Médéa	President
REBHI Redha	MCA.	Université de Médéa	Supervisor
KEZRANE Mohamed	Prof.	Université de Médéa	Co-Supervisor
ELMOHRI Abdennour	MCA.	Université de Médéa	Examiner
BENSEDIRA Sidali	MCA	Université de Blida	Examiner

Academic year : 2025-2026

Acknowledgment

Praise be to Almighty God, whose blessings of faith, courage, and patience have guided me throughout this journey.

I extend my deepest gratitude to my supervisor, Dr. REBHI Redha from. Yahya Fares Medea University, for his insightful guidance, unwavering support, and dedication, which have been instrumental to the success of this work.

I would like to express my heartfelt gratitude to my co-supervisor, Prof. KEZRANE Mohamed, from. Yahya Fares Medea University, for his invaluable guidance and support at the beginning of my research journey.

I would like to express my deepest gratitude to Prof. CHIBA Younes from the University of Medea for honoring me by presiding over the jury for this work.

I also extend my heartfelt thanks to the jury members. I would also like to express my sincere thanks to the members of the jury, Dr. ***ELMOHRI Abdennour****, Associate Professor (Class A) at the University of Medea, as well as Dr.* ***BENSEDIRA Sidali****, Associate Professor (Class A) at the University of Blida, for kindly agreeing to review.*

I am also sincerely thankful to the Doctoral Formation Committee for their steadfast support during my training.

The work presented in this manuscript was carried out within the Laboratory of Physical Mechanics and Mathematical Modeling (LMP2M)

Lastly, I am profoundly grateful to all the teachers and professors who have inspired and guided me throughout my academic journey at Medea Universities and to everyone who has directly or indirectly contributed to the completion of this project.

Not forgetting the apple of my eye, my wife ***Grara Nadhira****, my beloved children* ***Kamar Salam*** *and* ***Mabrouk Zayd Al-Khair****, my dear and respected parents - may God grant them long life - and all my family.*

Abstract

In the thermal spraying process studied, a molten aluminum particle is projected at high speed and flattens upon impact with a substrate. This phenomenon is modeled and simulated thermomechanical using the explicit software Abaqus. In this approach, the thermomechanical properties of the particle and substrate are considered temperature-dependent, and the study incorporates the three modes of heat transfer, accounting for a variable thermal contact conductance. First, the proposed model is compared with experimental data and numerical results reported in the literature. During the impact, the temporal evolution of the temperature of both the substrate and the droplet is analyzed. Additionally, the thickness of the solidified region of the molten droplet upon contact with the substrate is evaluated as a function of the substrate material, the initial droplet velocity, and the initial temperature of the substrate. Furthermore, the proposed model, which accounts for the thermal and mechanical interactions between the particle and the substrate, has proven to be valuable in deepening the understanding of the lamella formation mechanism and thermal transfer phenomena during the thermal spraying process

Keywords: Thermal spraying, thermomechanical, heat transfer, conductance, solidification, molten droplet.

Résumé

Dans le procédé de projection thermique étudié, une particule d'aluminium fondue est projetée à grande vitesse et s'aplatit lors de son impact avec un substrat. Ce phénomène est modélisé et simulé de manière thermomécanique à l'aide du logiciel explicite Abaqus. Dans cette approche, les propriétés thermomécaniques de la particule et du substrat sont considérées comme dépendantes de la température, et l'étude prend en compte les trois modes de transfert de chaleur, intégrant une conductance thermique de contact variable. Dans un premier temps, le modèle proposé est comparé aux données expérimentales et aux résultats numériques issus de la littérature. Lors de l'impact, l'évolution temporelle de la température du substrat et de la gouttelette est analysée. De plus, l'épaisseur de la zone solidifiée de la gouttelette fondue au contact du substrat est évaluée en fonction du matériau du substrat, de la vitesse initiale de la gouttelette et de la température initiale du substrat. En outre, le modèle proposé, qui prend en

compte les interactions thermiques et mécaniques entre la particule et le substrat, s'est révélé pertinent pour approfondir la compréhension du mécanisme de formation de la lamelle ainsi que des phénomènes de transfert thermique lors du processus de projection thermique.

Mots clés : Projection thermique, thermomécanique, transfert de chaleur, conductance, solidification, gouttelette fondue.

ملخص

في عملية الرش الحراري المدروسة، يتم قذف جسيم من الألمنيوم المنصهر بسرعة عالية وينبسط عند اصطدامه بالركيزة. يتم نمذجة هذا الظاهرة ومحاكاتها بطريقة حرارية-ميكانيكية باستخدام برنامج Abaqus الصريح. في هذا النهج، تُعتبر الخصائص الحرارية والميكانيكية للجسيم والركيزة معتمدة على درجة الحرارة، وتشمل الدراسة أوضاع انتقال الحرارة الثلاثة مع أخذ التوصيل الحراري المتغير للتلامس بعين الاعتبار. في البداية، يُقارن النموذج المقترح بالبيانات التجريبية والنتائج الرقمية المأخوذة من الأدبيات العلمية. خلال الاصطدام، يتم تحليل التطور الزمني لدرجة حرارة كل من الركيزة والقطيرة. بالإضافة إلى ذلك، يتم تقييم سمك المنطقة المتصلبة من القطيرة المنصهرة عند ملامستها للركيزة حسب مادة الركيزة، والسرعة الابتدائية للقطيرة، ودرجة الحرارة الابتدائية للركيزة. علاوة على ذلك، أثبت النموذج المقترح، الذي يأخذ في الاعتبار التفاعلات الحرارية والميكانيكية بين الجسيم والركيزة، فعاليته في تعميق فهم آلية تكوين الطبقة وأيضًا ظواهر انتقال الحرارة خلال عملية الرش الحراري.

كلمات مفتاحية: الرش الحراري، الحراري-الميكانيكي، انتقال الحرارة، التوصيلية، التصلب، والقطيرة المنصهرة.

Contents

Acknowledgment .....

Abstract .....

Résumé .....

List of Figures .....

List of Tables .....

List of Symbols .....

I.General Introduction……1

I.1 Introduction…… 1

I.1 Problematic Statement……1

I.3 Motivation 3

I.4 Contribution 3

I.5 Organization of the Manuscript 4

II. Literature Review ……..……..5

II.1 Historical Background of Thermal Spraying 6

II.2 The Various Thermal Methods. 7

II.3 Electric arc spraying 8

II.3.1 arc plasma principle: 8

II.3.2 The energy of the plasma: 8

II.4 Electric Arc Wire Spraying 9

II.5 Detonation Gun Spraying 9

II.6 Plasma Spraying 10

II.6.1 Principle of Plasma Spraying 11

II.6.2 Heat source 11

II.6.3 Parameters influencing spraying 11

II.7 Types of Plasma Spray Processes 11

II.7.1 HVOF (High Velocity Oxy-Fuel) 11

II.7.2 Cold spray 12

II.7.3 Flame spraying 13

II.7.4 Hypersonic Flame Spraying 14

II.8 The Substrate 15

II.8.1 Substrate Surface Preparation 15

II.8.2 Cleaning of the Work Piece Before Spraying 15

II.9 Coating Build-Up 16

II.10 Spraying Materials 16
II.11 Stainless Steel: Properties, Applications, and Binary Phase Diagrams: 16
II.11.1 Characteristics of Stainless Steel. 16
II.11.2 Uses and Applications 17
II.11.3 Iron-Carbon Binary Diagram 17
II.12 Copper: Properties, Applications, and Binary Phase Diagrams 18
II.12.1 Physical Properties 18
II.12.2 Mechanical Properties 18
II.12.3 Chemical Properties 18
II.12.4 Uses and Applications 18
II.12.5 Binary Phase Diagrams 19
III. Numerical Simulation ……20
III.1.Physical Model and Mathematical Formulation **……20**
III.1.1 Introduction 21
III.1.2 Physical model. 22
III.1.3. Mathematical model……..21
III.2. Numerical method…… …….24
III.2.1. Introduction 24
III.2.2. Grid mesh……..25
III.2.3. Validation……..26
IV.RESULTS AND DISCUSSION…… 31
IV.1 Introduction 32
IV.2 First section, a single particle 33
IV.2.1 Stainless-steel substrate 33
IV.2.2 Cooper substrate 37
IV.2.3 Nickel substrate 43
IV.3 Second Section, a Multiparticle System. 55
IV.4 Third Section: Elliptical Shape of the Droplet 58
IV.5 Conclusion: 66
IV.6 General Conclusion 67
IV.7 Perspectives 69
Bibliography : 70
List of Publication and Communication 73
International Publication…… ……73

National Conference:..... 73
International Conference:..... 734

List of Figures

Figure II.1 : Working principle of thermal spraying …… ……7

Figure II.2. Principle of Arc Plasma…….……. ……8

Figure II.3. Schematic representation of the operating principle of a detonation spraying gun (detonation gun)……..... ……9

Figure II.4. Schematic representation of the operating principle of a plasma torch…….. ……9

Figure II.5. Principle of a High Velocity Oxy-Fuel (HVOF) torch……. …...12

Figure II.6. Schematic diagram of a cold spray system…….. …...13

Figure II.7. Schematic representation of the Powder Flame Spraying process…….. …...14

Figure II.8. schematic representation of the wire Flame Spraying process……..... …..14

Figure II.9. Schematic representation of the Hypersonic Flame Spraying……..... …..15

Figure II.10. iron-carbon phase diagram……... …..17

Figure II.11. Binary Phase Diagram of Copper-Zinc Alloys (Brass System)…… …..19

Figure II.12. Binary Phase Diagram of Copper-Tin Alloys (Bronze System)…….. …..19

Figure II.13. Binary Phase Diagram of Copper-Nickel Alloys…….. ……20

Figure III.1. Thermal spray processes and physical model under analysis…….. ……22

Figure III.2. Magnetisation Grid of Sensitivity of Mesh…….. ……26

Figure III.3. A tin droplet's spread factor changes at (a) $T_w = 25°c$ &(b) $T_w = 150°c$ on a stainless steel substrate……. ……29

Figure III.4. Temperature evolution at the impact point of a tin droplet on a stainless-steel substrate at two initial wall temperatures: (a) Tw = 25 °C and (b) Tw = 150 °C… …...30

Figure III.5. Evolution of the spread factor for a tin droplet impacting an aluminum substrate (substrate temperature Tw = 26 °C, droplet temperature TD = 267 °C, droplet diameter D = 3.7 mm, and impact velocity U = 2.48 m/s)…….. ……30

Figure III.6. . Evolution of the dimensionless central splat height for the high-speed impact and contact (HSIC) of a copper droplet on a copper substrate. The simulation parameters are: droplet temperature (T_d= 1531 K), substrate temperature (T_w= 295 K), impact velocity (U = 2.52 m·s⁻¹), and droplet diameter (D = 4.67 mm)… ……29

Figure IV.1. Thermal response of an aluminum droplet impacting a stainless-steel substrate at varying wall temperatures ($U = 150\ ms^{-1}$)…… ……34

Figure IV.2. Transient temperature evolution at the impact point of a stainless-steel substrate by an Aluminum droplet at various initial substrate temperatures ($U = 150\ ms^{-1}$) ……35

Figure IV.3. Transient Thermal Behavior of an Aluminum Droplet Impacting stainless-steel substrates at Different Initial Temperatures (U = 100 m·s⁻¹)…… ……35

Figure IV.4. Time-Dependent Temperature Evolution at the Impact Site of a Stainless-Steel Substrate Subjected to Aluminum Droplet Deposition (U = 100 m·s⁻¹)…….. ……3
Figure IV.5. Transient Temperature Dynamics of an Aluminum Droplet Impacting Copper Substrates under Varying Preheating Conditions (U = 100 m·s⁻¹)…….. ……38
Figure IV.6. Transient Temperature Dynamics of an Aluminum Droplet Impacting Copper Substrates under Varying Preheating Conditions (U = 100 m·s⁻¹)…….. ……38
Figure IV.7. Time-Dependent Temperature Evolution at the Impact Site of a cooper Substrate Subjected to Aluminum Droplet Deposition (U = 100 m·s⁻¹)…….. ……40
Figure IV.8. Time-Dependent Temperature Evolution at the Impact Site of a cooper Substrate Subjected to Aluminum Droplet Deposition (U = 150 m·s⁻¹)……. ……41
Figure IV.9. Transient Variation of Solidification Thickness of an Aluminum Droplet Impacting a Copper Substrate at 100 m·s⁻¹ under Different Substrate Temperatures…….. ……43
Figure IV.10. Transient Variation of Solidification Thickness of an Aluminum Droplet Impacting a Copper Substrate at 100 m·s⁻¹ under Different Substrate Temperature…….. ……43
Figure IV.11. Temperature evolution of a droplet of aluminum impacting an nickel substrate at U = 100 m·s⁻¹ for different initial temperatures…….. ...….45
Figure IV.12. Temperature evolution of a droplet of aluminum impacting on nickel substrate at U = 150 m·s⁻¹ for different initial temperatures……. ……45
Figure IV.13. Transient Thermal Response of a Nickel Substrate Under Aluminum Droplet Impact (U = 100 m·s⁻¹)…….. ……47
Figure IV.14. Time-Resolved Heating Dynamics of a Copper Substrate Following Aluminum Droplet Impact (U = 150 m·s⁻¹)…….. ……47
Figure IV.15. Transient Solidification Behavior of an Aluminum Droplet on a Nickel Substrate at 100 m·s⁻¹ for Different Initial Substrate Temperatures…….. ……48
Figure IV.16. Transient Thermal Influence on the Solidification Thickness of Aluminum Droplets Impacting a Copper Substrate at 150 m·s⁻¹…… ……49
Figure IV.17. Temperature contour distribution for varying substrate temperatures…… ……50
Figure IV.18. Temperature change over time of an aluminum droplet on a stainless steel substrate at different impact velocities, Tw=25°C……. ……51
Figure IV.19. Changes in the thickness of the solidified layer over time of an aluminum droplet striking a stainless steel substrate at various speeds (Tw=25°C)…….. ……51
Figure IV.20. Stainless-steel substrate's temperature changes over time when aluminum droplets strike it at different speeds (Tw=25°C)……... ……51

Figure IV.21. Temporal evolution of the temperature of substrates of different grades subjected to aluminum droplet impact…… ……53
Figure IV.22. Temporal evolution of the temperature of an aluminum droplet impacting various substrate materials ($U = 150\, ms^{-1}, T_w = 25\, °C$)……. ……53
Figure IV.23. Temperature contour distribution for various substrate grades……. ……54
Figure IV.24. Evolution of the solidification thickness of an Aluminum droplet on a stainless-steel substrate at variable temperatures…….. ……55
Figure IV.25. Evolution of the solidification thickness of an Aluminum droplet on Substrates of varying grades…… ……55
Figure IV.26. Temperature Contour Mapping for a Multi-Particle Impacts…… ……57
Figure IV.27. Temporal variation of substrate temperature during the impact of three particles….. ……58
Figure IV.28. Evolution of the Temperature of a Stainless-Steel Substrate (T_0 = 25 °C) During the Impact of an Elliptical Aluminum Particle at 150 m/s…… ……60
Figure IV.29. Temperature Evolution of an Elliptical Aluminum Particle Impacting a Stainless-Steel Substrate (T_0 = 25 °C) at 150 m/s…….. ……61
Figure IV.30. . Temporal Evolution of the Thickness of a Solidified Elliptical Aluminum Droplet on a Stainless-Steel Substrate (T_0 = 25 °C) During Impact at 150 m/s…… ……62
Figure IV.31. . Comparison of Temperature Evolution of a Stainless-Steel Substrate During the Impact of Two Aluminum Particles at 150 m/s……. ……63
Figure IV.32. Temperature Decay of Elliptical and Spherical Aluminum Droplets During Impact on a Stainless-Steel Substrate at 150 m/s…… ……64
Figure IV.33. Comparison of Solidified Thickness Evolution of Elliptical and Spherical Aluminum Droplets Impacting a Stainless-Steel Substrate at 150 m/s……. ……65
Figure IV.34. Temperature Contours Generated by the Impact of an Elliptical Particle…….. ……66

List of Tables

Table II 1. Comparative summary table of the stable and metastable iron–carbon (Fe–C) phase diagrams…… …...16

List of symbols

$\boldsymbol{T_w}$	Substrate Temperature.	°c
$\boldsymbol{T_d}$	Droplet Temperature.	°c
t	Time	s
s	Second.	s
D	Diameter.	mm
m	Meter.	M
U	Velocity.	ms^{-1}
$\boldsymbol{\theta^N}$	Nodal Temperature	°c
$\boldsymbol{i}$	The Increment Index	integer
$\mathbf{F^J}$	Internal Flux Vector	wm^{-2}
$\mathbf{C^{NJ}}$	Lumped Capacitance Matrix	Jk^{-1}
$\mathbf{P^J}$	Nodal Source Vector	w
$[\boldsymbol{C}]$	The Capacitance Matrix	J/K
$\boldsymbol{C_p(T)}$	Specific Heat Capacity	J/(kg·K)
$\boldsymbol{H_f}$	Latent Heat Of Fusion	J/kg
$\boldsymbol{T_{sol}}$	Solidus	°c
$\boldsymbol{T_{liq}}$	Liquidus	°c
$\boldsymbol{\mu^{.N}}$	Degree of Freedom	integer
$\mathbf{P_H}$	Hugoniot Pressure	Pa
$\mathbf{E_H}$	Hugoniot Energy	J/kg
η	Nominal Compressive Strain	integer
$\boldsymbol{\mu_0}$	Pre-Exponential Factor	m^2/s
E	Activation Energy For Viscous Flow	J/mol
R	Universal Gas Constant	J/(mol·K)

CHAPTER I GENERAL INTRODUCTION

I.1. INTRODUCTION

In almost every modern industrial field, the durability and performance of materials are a major concern. Whether in aerospace turbines exposed to extreme temperatures, automotive components subjected to wear, or biomedical implants requiring excellent biocompatibility, the surface quality often determines the reliability of the entire system. To meet these demands, thermal spraying has emerged as an essential technology. It offers the ability to modify the surface of materials by depositing a protective or functional coating, without altering the intrinsic properties of the substrate.

In simple terms, the principle is straight forward: metallic or ceramic particles are melted and then propelled at high velocity to impact a surface, where they progressively build up a coating. Yet, behind this apparent simplicity lies a much more complex reality. Each particle follows a unique trajectory: heated in a thermal jet and accelerated at high speed, it impacts the substrate, deforms, spreads, rapidly cools within microseconds, and contributes to the formation of a microstructure with specific properties. These ultra-fast phenomena, invisible to the naked eye, directly determine the final quality and performance of the coating.

Studying and controlling such a process exclusively through experiments is a real challenge. On the one hand, spraying conditions vary greatly depending on the material, the substrate, and the process used. On the other hand, each trial is costly: powders and gases are expensive, and spraying facilities require considerable investment. Moreover, it is simply impossible to experimentally reproduce all possible combinations of parameters. This severely limits the ability of engineers and researchers to systematically optimize the process.

This is precisely where numerical simulation becomes a vital tool. It allows us to dive virtually in to the heart of the process, observe what is beyond the reach of experimental instruments, and test a wide range of configurations quickly and at reduced cost. Through modeling, one can visualize the particle trajectory, understand its behavior upon impact, predict solidification, and anticipate the development of residual stresses. Simulation therefore provides a valuable framework for linking operating parameters to microstructure and, ultimately, to the coating’s properties.

Among the available simulation tools, ABAQUS/CAE holds a privileged position. Its ability to handle coupled thermo-mechanical phenomena as well as fast dynamic events makes it perfectly suited for modeling particle behavior during thermal spraying. Using this software, it becomes possible to represent the impact of molten particles on a substrate with great accuracy, analyze their spreading and cooling, and predict the stresses induced within the deposit. More broadly, ABAQUS provides a flexible environment that facilitates parametric exploration and process optimization.

The aim of this thesis is therefore clear: to contribute to a better understanding of the thermal spraying process through advanced numerical simulation. By relying on ABAQUS/CAE, we seek to establish reliable models capable of accurately reproducing the physical phenomena involved, while providing practical insights to improve coating quality. By reducing the dependence on costly experiments and offering a more complete view of the process, this approach paves the way for the design of innovative coatings tailored to the growing demands of modern industry.

I.2. PROBLEMATIC STATEMENT

In the thermal spraying process under investigation, a molten aluminum particle is propelled at supersonic velocity and undergoes significant deformation upon impact with the substrate, spreading into a thin lamella. This complex phenomenon is captured through a thermomechanical modeling approach using the explicit solver of Abaqus. The simulation accounts for the three fundamental modes of heat transfer (conduction, convection, and radiation) by integrating a variable thermal contact conductance that evolves dynamically with temperature and contact conditions. Both the particle and the substrate are characterized by thermomechanical properties that are explicitly treated as temperature-dependent, thereby enhancing the realism of the computational model.

To ensure reliability, the proposed model is validated against both experimental observations and previously reported numerical studies, demonstrating its robustness in predicting particle substrate interactions. The temporal evolution of temperature within the droplet and the substrate is carefully monitored throughout the impact process, highlighting the strong coupling between thermal and mechanical responses. Key parameters (including the initial droplet velocity, the preheating level of the substrate, and the intrinsic material properties of the substrate) are shown to exert a direct influence on the thickness and morphology of the solidified splat formed upon impact.

By explicitly considering the interplay between thermal diffusion, plastic deformation, and solidification kinetics, the model provides deeper insight into the mechanisms governing lamella formation in thermal spray coatings. This allows for a better understanding of how process conditions affect coating adhesion, microstructural development, and ultimately, the functional performance of thermally sprayed layers. Beyond its predictive capability, the model serves as a valuable tool for optimizing spray parameters and tailoring coating properties for specific industrial applications

I.3. MOTIVATION

Thermal spraying has emerged as a versatile surface engineering technique, widely applied in aerospace, energy, and biomedical industries due to its ability to produce protective coatings with tailored properties. However, the underlying physics of droplet impact, solidification, and adhesion remain highly complex and are influenced by a wide range of parameters such as particle velocity, substrate temperature, and material characteristics. A fundamental understanding of these mechanisms is essential for improving coating performance, optimizing process parameters, and reducing experimental costs.

Despite significant experimental advances, many aspects of splat formation and lamella evolution cannot be easily captured in practice due to the extremely short time scales and high temperatures involved. Numerical modeling therefore plays a crucial role in bridging this gap, enabling researchers to simulate particle–substrate interactions and explore the thermomechanical phenomena that govern coating adhesion and microstructure development.

The motivation of this study lies in providing a reliable thermomechanical model that captures the coupled heat transfer and mechanical deformation during droplet impact. Such a model not only enhances the predictive capability of thermal spray simulations but also contributes to a deeper scientific understanding of coating formation mechanisms. Ultimately, this knowledge can guide the optimization of industrial processes, leading to coatings with improved durability, functionality, and efficiency in demanding applications.

I.4.CONTRIBUTION

The present study contributes to the field of thermal spraying by developing and validating a comprehensive thermomechanical model of molten droplet impact on a solid substrate. Unlike conventional approaches, the proposed framework simultaneously accounts

for variable thermal contact conductance, temperature dependent material properties, and the combined effects of heat transfer and mechanical deformation during impact. This integration provides a more realistic representation of splat formation and lamella evolution.

The model is systematically validated through comparison with both experimental observations and previously published numerical results, thereby ensuring its robustness and reliability. By analyzing the influence of key parameters (such as droplet velocity, substrate preheating, and substrate material properties) on the morphology and thickness of the solidified layer, the study offers valuable insights into the mechanisms that govern coating adhesion and microstructural development.

Furthermore, the methodology developed in this work establishes a predictive tool that can be applied to optimize process parameters in industrial thermal spraying. Beyond its practical relevance, the study also advances the scientific understanding of droplet–substrate interactions at high temperatures and short time scales. As such, it bridges the gap between experimental limitations and industrial requirements, contributing both to fundamental research and technological innovation in surface engineering.

I.5. ORGANIZATION OF THE MANUSCRIPT

This thesis is structured into several chapters, each addressing a key aspect of the study. The first chapter provides a general introduction, emphasizing the growing importance of thermal spraying in modern industry and outlining the technological progress that has accompanied its development.

The second chapter offers a comprehensive literature review, presenting the different thermal spray processes, their operating principles, performance characteristics, and industrial applications. This chapter also highlights the main scientific contributions and current challenges in the field.

The third chapter is devoted to the development of the physical model and the corresponding mathematical formulation, which form the foundation of the numerical analysis.

The fourth chapter focuses on the numerical simulation**,** describing in detail the modeling approach, assumptions, boundary conditions, and computational parameters used.

The fifth chapter presents and discusses the obtained results, providing a critical interpretation of the findings and linking them to the objectives of the study.

Finally, the last chapter summarizes the main conclusions of this research and proposes future perspectives, aiming to guide further investigations and improvements in this field.

CHAPTER II LITERATURE REVIEW

II.1. HISTORICAL BACKGROUND OF THERMAL SPRAYING

Thermal spraying is a surface treatment process used to produce functional or protective coatings. Its operation is based on several fundamental principles:

- The melting of the feedstock material is achieved through the action of a thermal jet.
- The acceleration of the molten or semi-molten material (in powder or wire form) to ensure optimal spreading and, consequently, effective adhesion of the particles to the substrate.

Several spraying techniques exist, enabling the attainment of coating properties tailored for the deposition of high-quality layers, while ensuring the desired characteristics of the coating. These thermal processes utilize velocities and temperatures tailored to the properties of the sprayed particles as illustrated in Figure II.1.

Most materials can be melted using thermal spraying, including refractory materials. However, for temperature-sensitive substances such as those prone to oxidation or structural changes in their crystalline form the impact of particles can generate significant thermal gradients. These high temperatures may severely alter the properties of the feedstock material, thereby compromising the integrity, adhesion, and overall performance of the final coating.

To address these thermal limitations and broaden the range of applications and coating materials in thermal spraying, alternative processes have been developed. The HVOF (High Velocity Oxygen Fuel) process, for instance, is a high-velocity flame spraying technique that exposes particles to lower temperatures compared to plasma spraying approximately 2,000 °C in the case of HVOF, versus 3,000 °C for plasma spraying, The HVOF process is also characterized by significantly higher particle velocities ranging from 600 to 800 m/s, compared to approximately 250 m/s in plasma spraying. In this process, the powder is not only melted but also highly accelerated, resulting in dense, hard coatings with excellent adhesion to the substrate. Moreover, the relatively lower temperatures of the HVOF technique help minimize oxidation and decarburization issues commonly observed when spraying sensitive materials such as metal powders or carbides.

A cold spraying technique, known as *Cold Spray* [1], has also been developed to mitigate thermal issues related to the melting of feedstock materials. This process is characterized by the absence of a thermal energy source. The principle of *Cold Spray* involves accelerating a compressed gas through a nozzle to supersonic velocities around 1000 m/s. The material to be deposited is introduced into the high-pressure section of the nozzle (20, 30 bar) and is propelled in a solid, unmelted state toward the substrate.

This process offers numerous advantages due to its unique spraying conditions and has experienced significant development in recent years [2].

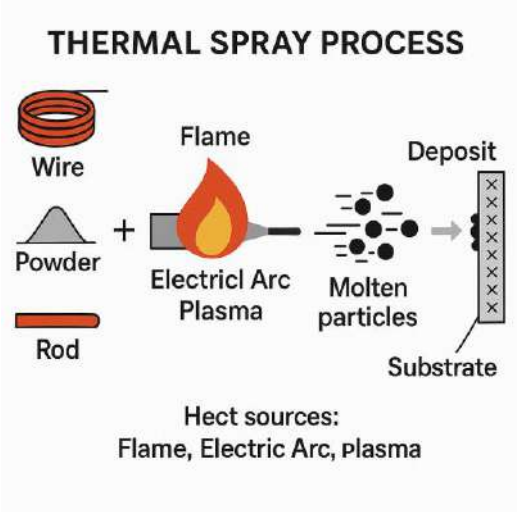


Figure II.1. Working principle of thermal spraying. [1]

II.2. THE VARIOUS THERMAL METHODS.

Several thermal spraying methods can be identified, typically classified based on the energy source used and the specific spraying conditions applied.

- Electric arc spraying
- Detonation spraying
- Plasma spraying
- H.V.O.F spraying (High Velocity Oxy-Fuel)
- Cold spray
- flame spraying
- Powder flame spraying

II.3. ELECTRIC ARC SPRAYING

II.3.1 ARC PLASMA PRINCIPLE:

Arc plasma (Figure II.2) refers to a highly dissociated and ionized atmosphere that conducts electric current. It replaces the terms *plasma flame* or *plasma jet*. The application of arc plasma is not new [3]; it has been widely used in high-temperature welding, such as in the flame of atomic hydrogen torches, which are rich in plasma. The energy of the plasma is only meaningful if it is controlled and directed a concept developed by the German researcher H. Gerdein in the 1920s Arc plasma relies on a heat source known as thermal plasma, generated by the partial ionization of a plasma-forming gas. When the gas reaches the plasma state, it produces extremely high temperatures. A key feature of this spraying system is the intense constriction applied to the arc, allowing the plasma to reach temperatures ranging from 10,000 to 15,000 °C. Such temperatures are sufficient to melt virtually all materials, including the most refractory ones.

The gas flow at the nozzle exit, taking into account its expansion, can reach very high ejection velocities (often exceeding the speed of sound). These velocities range between 800 and 1200 m/s, depending on the plasma density and the type of gas used. Such conditions enable good melting and effective spreading of the particles upon impact with the substrate.

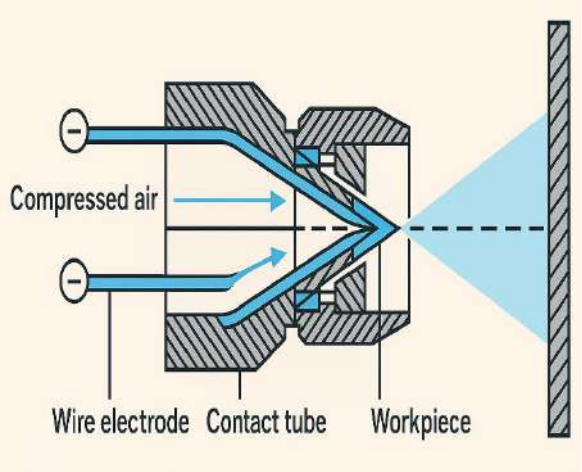


Figure II.2. Principle of Arc Plasma. [1]

II.3.2.THE ENERGY OF THE PLASMA:

The energy supplied and the temperature reached during arc plasma processing depend on the following factors:

The energy supplied and the temperature reached during arc plasma processing depend on:

- The electrical power supplied to the source,

- The mass flow rate,
- The nature of the plasma-forming gas,
- The geometry of the torch *(including the internal diameter, anode shape, and gas injection method).*

The energy contained in the gas is released differently with increasing heat, depending on whether the gas is diatomic or monoatomic. If a high energy content at moderate temperature is desired, diatomic gases such as nitrogen or hydrogen are preferred. Conversely, if a high temperature is required, monoatomic gases like argon or helium are chosen.

Arc plasma can use water as a plasma medium, as it dissociates within the arc to produce a hydrogen-rich plasma, resulting in power levels significantly higher than those obtained with gas-based plasmas.

II.4. ELECTRIC ARC WIRE SPRAYING

This process involves generating an electric arc between two consumable wire electrodes made of ductile, conductive materials, which act both as the heat source and the feedstock The heat from the arc melts the wire tips, which are then atomized into fine droplets and propelled onto the substrate by a stream of compressed air.

Electric arc spray guns are powered by direct current (DC) generators, operating at arc voltages between 25 and 40 V, with currents ranging from 100 to 500 A. This spraying method is simple, cost-effective, and efficient, but it is restricted to electrically conductive materials that can be drawn into wire form. However, the recent development of cored ceramic wires is expanding the applicability of this process. [3, 4]

II.5. DETONATION GUN SPRAYING

In this process, the feedstock material in powder form is injected into a sealed tube known as a detonation gun (see Figure II.3), along with a combustible gas mixture typically oxygen and acetylene.

This mixture is ignited by a spark at a frequency of 6 to 8 detonations per second, generating an explosion. The resulting shockwave, with an overpressure of approximately 2 MPa, heats and propels the powder particles at extremely high velocity (up to 950 m/s) toward the substrate.

This is a discontinuous process, requiring purging with an inert gas between each detonation. The coatings produced exhibit exceptional properties, including:

- Porosity below then 1%.
- Adhesion strength exceeding 80 MPa.
- Deposition rates between 3 and 5 kg/h [3].

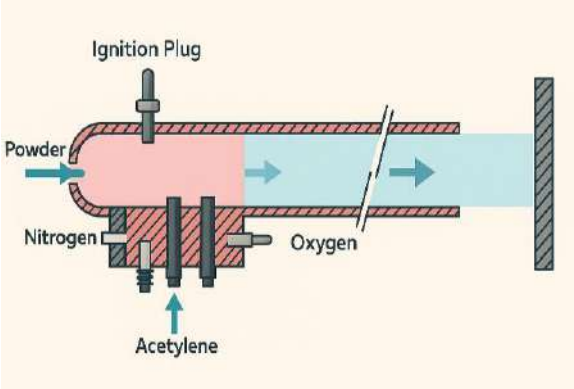


Figure II.3. Schematic representation of the operating principle of a detonation spraying gun (detonation gun). [2]

II.6. PLASMA SPRAYING

Plasma is considered the fourth state of matter. It is an ionized gas consisting of a mixture of molecules, atoms, ions, and electrons, which as a whole remains electrically neutral [1, 5]. Generating plasma requires three essential components:

- A power supply (DC generator)
- A gas ionization system (typically a high-frequency or high-voltage discharge)
- A coupling mechanism that enables current flow between two electrodes through the ionized gas.

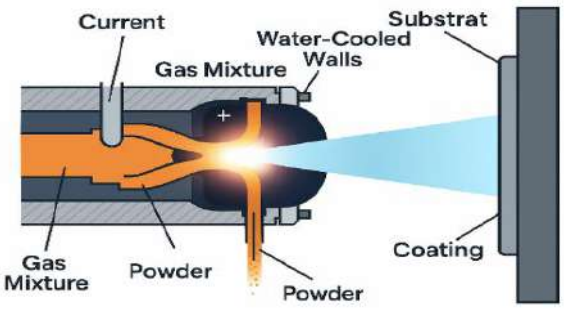


Figure II.4. Schematic representation of the operating principle of a plasma torch. [3]

II.6.1. PRINCIPLE OF PLASMA SPRAYING

This technique was used to deposit the samples studied. It relies on a high-intensity electric arc (several hundred amperes) formed between two electrodes within an ionized gas stream, usually initiated by a high-frequency discharge (see Figure II.4).

The plasma-forming gas is heated to extremely high temperatures (between 15,000 and 20,000 °C) and accelerated through a nozzle**,** exiting at velocities ranging from 1000 to 1500 m/s [15].

The feedstock material**,** in powder form, is injected into this high-energy plasma jet using a carrier gas (typically argon). The powder particles are melted and propelled at high speed toward the substrate to form a coating [1, 2, 9].

II.6.2. HEAT SOURCE

The heat source must deliver sufficient energy to allow the feedstock material to reach its melting point (thermal transfer) and to generate a gas jet capable of propelling the molten particles toward the substrate (kinetic transfer).

Both thermal and kinetic transfers govern the melting, spreading, and solidification of the particles, which in turn have a significant impact on the final coating properties. [2]

II.6.3. PARAMETERS INFLUENCING SPRAYING

The morphology and properties of the coatings produced by plasma spraying are strongly influenced by various experimental parameters, primarily related to:

- The type of feedstock material**,**
- The characteristics of the heat source,
- The surrounding atmosphere (gas composition, pressure, etc.),

II.7. TYPES OF PLASMA SPRAY PROCESSES

II.7.1. HVOF (HIGH VELOCITY OXY-FUEL)

The HVOF process also employs a flame torch, but its uniqueness lies in the use of a combustion chamber operating under pressures between 5 and 7 bar, followed by a convergent-divergent nozzle. This specific geometry enables the gas flow to reach supersonic velocities ranging from 1800 to 2200 m/s and flame temperatures between 2500°C and 2800°C (see Figure II.5). [2]

The feedstock material, typically in powder form, is injected into the flame using an inert carrier gas. The particles are melted or partially melted and accelerated through the nozzle, reaching velocities of 300 to 600 m/**s**. Due to the high internal pressure within the torch, acetylene cannot be used as a fuel gas because of the risk of explosion. [10–14] Despite their extremely short residence time in the flame (a few tenths of a millisecond), the particles reach a semi-molten state. The high kinetic energy they acquire enables the formation of high-quality coatings with the following characteristics:

- Low porosity (< 2%).
- Strong adhesion (70–100 MPa).
- Low surface roughness [1].

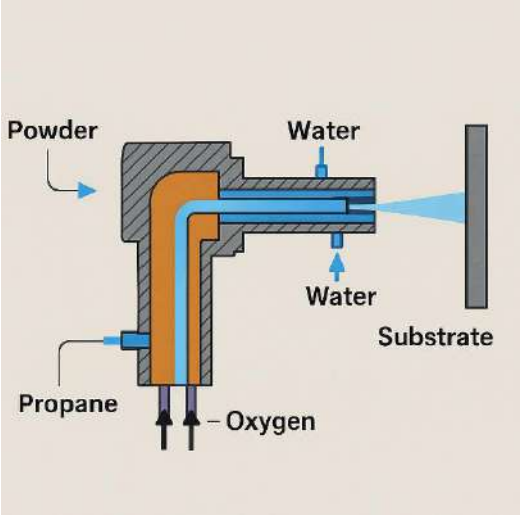


Figure II.5. Principle of a High Velocity Oxy-Fuel (HVOF) torch. [1]

II.7.2. COLD SPRAY

Cold spray is a coating technique that consists in projecting metallic or non-metallic materials at very high velocities (200–1200 m/s) onto a substrate. The particles used, with sizes ranging from 1 to 100 µm, are accelerated by a supersonic jet of compressed gas. The process relies on the optimal adjustment of temperature, particle velocity, and particle size, while ensuring that the operating temperature remains below the melting point of the feedstock material.

As a result, the coating is formed through the impact of solid-state particles, thereby avoiding or significantly reducing the detrimental effects associated with high temperatures, reactive gases, and other limitations of conventional thermal spray processes. The minimization

of thermal effects on both the coating and the substrate represents a major advantage, making cold spray a highly promising technique for a wide range of industrial applications [2,3,5].

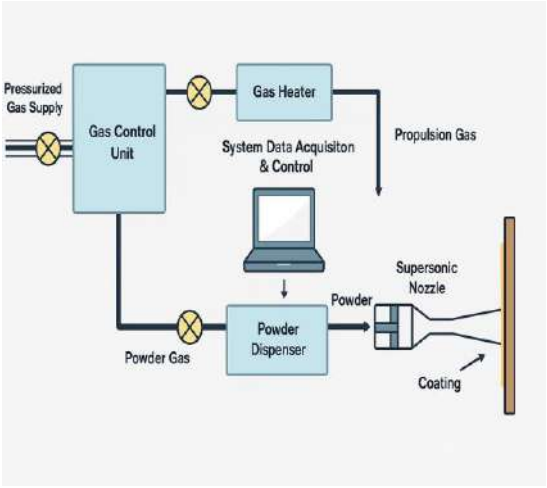


Figure II.6. Schematic diagram of a cold spray system. [1]

II.7.3. FLAME SPRAYING

refers to any thermal spray process that utilizes the thermal energy produced by the combustion of a fuel gas with oxygen. The temperature of an oxy-fuel flame typically ranges between 2800°C and 3150°C. Materials that melt below 2800°C and do not sublimate can be effectively deposited using this method.

Two main types of flame spraying exist, based on the form of feedstock: powder-based and wire-based.

II.7.3. POWDER FLAME SPRAYING

Powder flame spraying is the oldest thermal spray technique, involving the injection of a powdered material into an oxy-fuel flame. The powder is partially or fully melted and propelled toward the substrate by the kinetic energy of the combustion gases (see Fig. II.8) [,]. Typical flame temperatures are around 3000°C. The particle velocity in standard flame spraying is relatively low (approximately 50 m/s), which often necessitates additional acceleration using auxiliary air jets. The stand-off distance (distance between the nozzle and the substrate) is generally between 100 mm and 200 mm, allowing sufficient dwell time for the powder particles to melt and adhere effectively to the substrate surface.

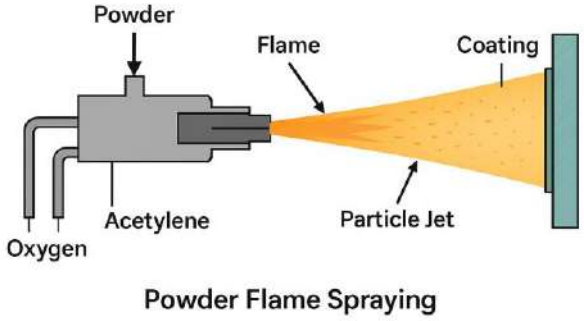


Figure II.7. Schematic representation of the Powder Flame Spraying process. [5]

II.7.4. WIRE FLAME SPRAYING

In this process (Figure II.8), the feedstock material is introduced into the center of the flame in the form of a wire, rod, or cord. the same fuel gases as in powder flame spraying (typically oxygen and acetylene) are used solely to melt the material. Once melted, the material is atomized by a stream of compressed air that propels the molten particles toward the substrate. The particle velocity reaches approximately 150 m/s, and the tip of the wire can reach up to 95% of the flame temperature**.** This technique allows for the deposition of certain ceramics at rates ranging from 1 kg/h to over 30 kg/h, depending on the material, the desired coating properties, and the wire or rod diameter. [2,5]

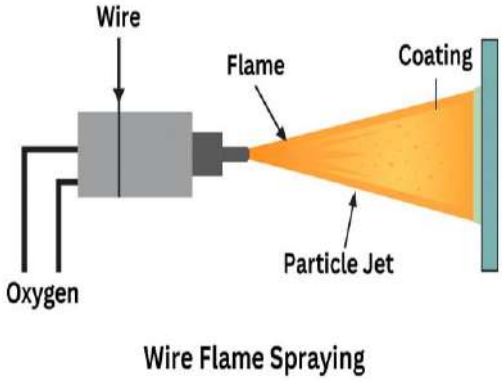


Figure II.8. schematic representation of the wire Flame Spraying process. [5]

II.7.5. HYPERSONIC FLAME SPRAYING

This spraying method derives its name from the extremely high exhaust gas velocity, which ranges between Mach 1 and Mach 2**.** It encompasses two main processes:

- Intermittent hypersonic spraying**:** *Detonation gun spraying.*
- Continuous hypersonic spraying**:** HVOF (High Velocity Oxy-Fuel)

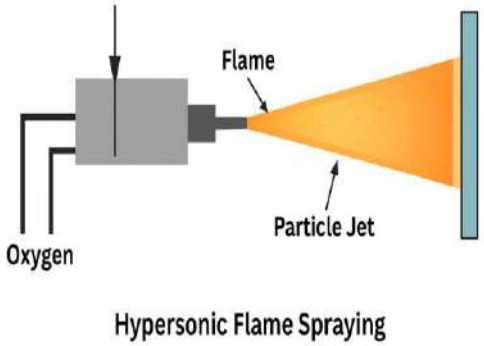


Figure II.9. Schematic representation of the Hypersonic Flame Spraying [1].

II.8. THE SUBSTRATE

The physicochemical condition of the substrate surface plays a critical role in the formation of the coating (lamellar structure) and, consequently, in its adhesion.
Adhesion is a key quality parameter, as it ensures proper bonding between the coating and the substrate.

II.8.1 SUBSTRATE SURFACE PREPARATION

Surface preparation is a necessary step prior to thermal spraying operations. It primarily involves:

- Creating surface roughness through a mechanical treatment known as abrasive blasting (or grit blasting), which promotes mechanical anchoring of molten or semi-molten particles by embedding them into the surface irregularities.
- This enhances the adhesion strength of the deposited coating.

II.8.2. CLEANING OF THE WORK PIECE BEFORE SPRAYING

Thorough cleaning of the work piece is essential to remove any contaminating substances such as grease, dust, or surface inclusions**.** This process is typically performed using ultrasonic cleaning or solvent-based treatments [1,2]. The cleaning agents used can include organic solvents or alkaline detergents**.**
It should be noted that abrasive blasting introduces compressive residual stresses near the treated surface.

II.9. COATING BUILD-UP

The formation of the coating is achieved through the impact**,** plastic deformation**,** rapid solidification, and successive layering of molten or semi-molten droplets on the substrate. The resulting structure is typically lamellar in nature [3, 6], and may contain oxides**,** micro-porosities**,** cracks, and contact zones between lamellae and with the substrate that vary in quality.

The manner in which the droplets spread and solidify has a significant effect on coating characteristics**,** particularly its porosity**.**

The mechanisms proposed in this thesis are relatively complex and depend on:

- the kinetic and thermal energy of the particles,
- their viscosity and wettability on the substrate,
- the nature, surface condition, and temperature of the substrate. [1,2,3]

II.10. SPRAYING MATERIALS

The most commonly used materials for protective coatings against corrosion and wear are alumina (Al_2O_3) and Ni-Al alloys. These materials are of significant technological interest due to their outstanding mechanical and thermal properties, including high strength and elevated melting points**.** They also exhibit excellent resistance to high-temperature corrosion**.**

II.11. STAINLESS STEEL: PROPERTIES, APPLICATIONS, AND BINARY PHASE DIAGRAMS:

II.11.1. CHARACTERISTICS OF STAINLESS STEEL.

PHYSICAL PROPERTIES

- ✓ Density: 7.7 – 8.0 g/cm^3.
- ✓ Melting Point: 1375 – 1530 °C (depending on the alloy)
- ✓ Thermal Conductivity: 15–25 W/(m*K).
- ✓ Magnetism: variable depending on the structure (austenitic non-magnetic, ferritic magnetic).

MECHANICAL PROPERTIES

- ✓ Tensile Strength**:** 500–1000 MPa (depending on grade and treatment)
- ✓ Elongation at Break: 20–40 %.
- ✓ Hardness: 150–600 HV depending on heat treatment.
- ✓ Ductility and Formability: good for certain grades

CHEMICAL PROPERTIES

- ✓ Excellent Corrosion Resistance: due to chromium content (Cr > 10.5 %)
- ✓ Resistance to Acids, Bases, and Oxidizing Atmospheres
- ✓ Formation of a Passive Chromium Oxide Layer that protects the metal.

II.11.2. USES AND APPLICATIONS

- Piping and Chemical Equipment.
- Food and Medical Tanks.
- Aerospace and Automotive Components.
- Construction and Architectural Equipment.
- Turbine Components and Heat Exchangers.

II.11.3. IRON-CARBON BINARY DIAGRAM

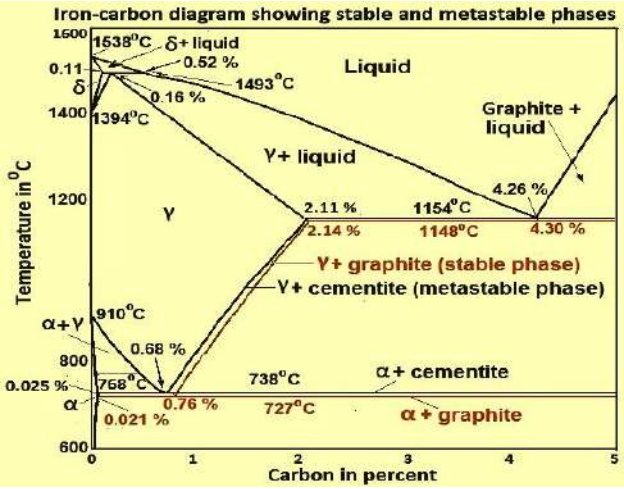


Figure II.10. iron-carbon phase diagram. [35]

Table II 1. Comparative summary table of the stable and metastable iron–carbon (Fe–C) phase diagrams. [35]

Criterion	Metastable Diagram (Fe–Fe_3C)	Stable Diagram (Fe–Graphite)
Predominant carbon phase	Cementite (Fe_3C)	Graphite (C)
Use / Practical Application	Common steels, steel microstructures (ferrite, austenite, pearlite, cementite)	Carbon-rich cast irons, graphite formation with slow cooling
Equilibrium conditions	Metastable equilibrium (cementite may decompose into Fe + graphite over time)	Thermodynamically stable equilibrium (Fe + graphite)
Carbon content range	0 % to ~6.67 % C	Mainly > 2 % C in cast irons

Practical representation	Mainly used for steel studies	Used for cast irons and graphite formation studies
Formation	Rapid, cementite forms during industrial cooling	Slow, graphite forms under very slow cooling conditions or with elements favoring graphitization

II.12. COPPER: PROPERTIES, APPLICATIONS, AND BINARY PHASE DIAGRAMS

II.12.1. PHYSICAL PROPERTIES

- ✓ Density: 8.96 g/cm³.
- ✓ Melting Point: 1084.62 °C.
- ✓ Thermal Conductivity: ~385 W/(m*K).
- ✓ Electrical Conductivity: Very high (~59.6×10^6 S/m).
- ✓ Color: Reddish metallic luster.
- ✓ Ductility & Malleability: Excellent.

II.12.2. MECHANICAL PROPERTIES

- ✓ Tensile Strength: 210–370 MPa (depending on processing and alloying)
- ✓ Yield Strength: 70–250 MPa
- ✓ Elongation at Break: 30–50 %
- ✓ Hardness: 40–120 HV
- ✓ Good corrosion resistance in many environments, though susceptible to acids and oxidizing agents

II.12.3. CHEMICAL PROPERTIES

- ✓ Corrosion Resistance: Forms a protective oxide layer (Cu_2O, CuO) in air
- ✓ Reaction with Acids: Reacts with oxidizing acids (e.g., HNO_3), less reactive with non-oxidizing acids.
- ✓ Alloying Behavior: Forms alloys with elements like Zn, Sn, Ni, Al, improving mechanical strength and corrosion resistance.

II.12.4. USES AND APPLICATIONS

- ✓ Electrical wiring and conductors.
- ✓ Plumbing and piping.
- ✓ Heat exchangers and radiators.
- ✓ Coins, decorative items, and jewelry.

- ✓ Industrial machinery components.
- ✓ Alloys: Brass (Cu-Zn), Bronze (Cu-Sn).

II.12.5. BINARY PHASE DIAGRAMS

Copper forms binary alloys with many metals. The most studied include:

- ✓ Copper-Zinc (Cu-Zn): Forms brass; shows α, β, γ phases depending on composition and temperature.
- ✓ Copper-Tin (Cu-Sn): Forms bronze; eutectic compositions and various intermetallic phases
- ✓ Copper-Nickel (Cu-Ni): Fully miscible, forms a continuous solid solution
- ✓ Copper-Aluminum (Cu-Al): Forms several intermetallic compounds (Cu_3Al, $CuAl_2$)

Binary phase diagrams help predict phase transformations, solubility limits, and microstructure evolution during alloying and heat treatment.

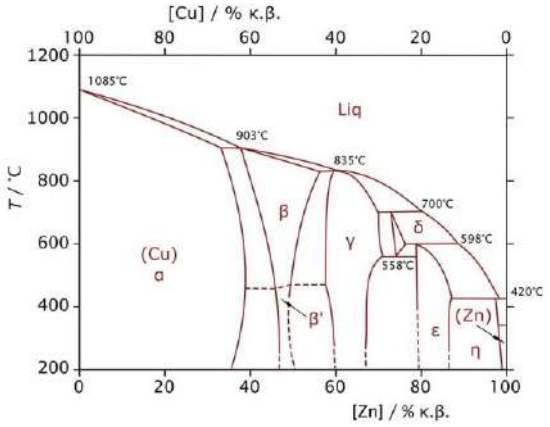


Figure II.11. Binary Phase Diagram of Copper-Zinc Alloys (Brass System). [36]

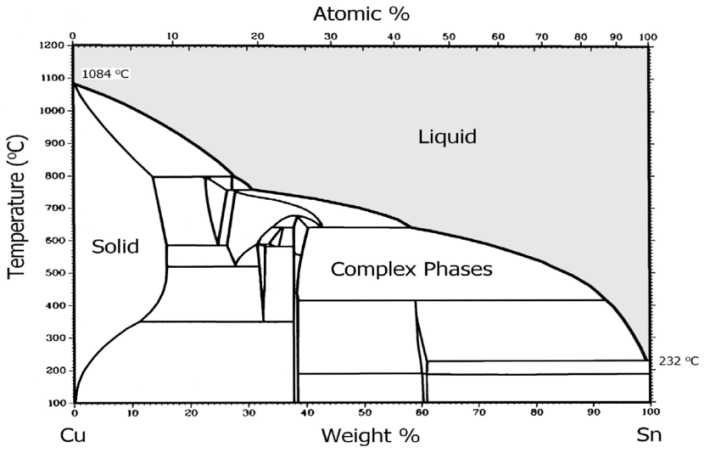


Figure II.12. Binary Phase Diagram of Copper-Tin Alloys (Bronze System) [36]

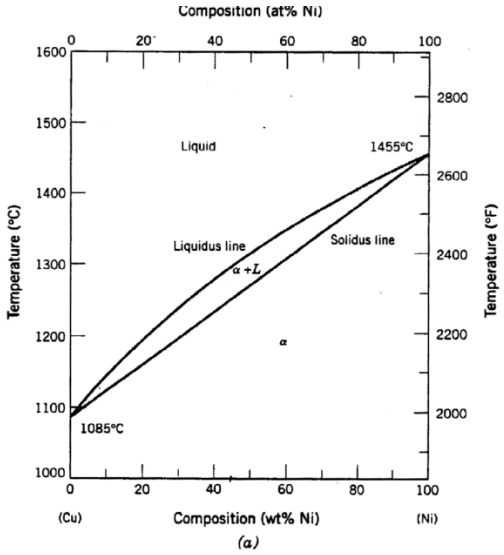


Figure II.13. Binary Phase Diagram of Copper-Nickel Alloys. [36]

CHAPTER III NUMERICAL SIMULATION

III.1. PHYSICAL MODEL AND MATHEMATICAL FORMULATION.

III.1.1. INTRODUCTION

Thermal spraying is an advanced coating technique that involves propelling by means of a controlled spray gun, molten or semi-molten particles toward a surface known as the substrate. The primary objective of this process is to build up, through the successive accumulation of sprayed particles, a protective layer with specific mechanical and functional properties. The success of this operation relies on the precise adjustment of several parameters, including the melting temperature of the particles, their acceleration velocity within the gas jet, and the angle of incidence at the moment of impact. By controlling these variables, it becomes possible to produce coatings that exhibit excellent adhesion to the substrate, homogeneous density, and performance tailored to the intended service conditions.

As illustrated in Figure III.1, the final quality of the coating strongly depends on the individual characteristics of the particles at the moment of impact. Particles of different sizes and geometries reach the target surface at varying velocities and incidence angles. This diversity generates a complex microstructure in which successive layers of material intertwine and solidify in a random yet complementary manner, thereby imparting the final properties to the coating. Consequently, the interaction between spraying parameters and particle properties determines not only the morphology of the deposited layer but also its performance in terms of hardness, wear resistance, oxidation protection, or even thermal and electrical conductivity.

Nevertheless, despite technological advancements, the simultaneous study of all these phenomena remains extremely complex, as it requires accounting for numerous dynamic and thermomechanical interactions. To better understand the fundamental mechanisms involved in coating formation, a commonly adopted approach consists of simplifying the analysis by focusing on the impact of a single particle on the substrate. This method makes it possible to isolate the thermal and mechanical effects associated with spreading, cooling, and solidification, and represents an essential step toward the comprehensive modeling of the process.

In the present study, attention is placed on the normal impact of a spherical molten droplet, as depicted in Figure 1. In this baseline configuration, the initial droplet diameter is

denoted as **D**, its initial temperature as $T_{droplet}$, the impact velocity as **U**, and the initial substrate temperature as **Tw**. This simplified representation has the advantage of highlighting the elementary phenomena that occur upon contact between a particle and the substrate: plastic deformation due to impact velocity, spreading into a disk-shaped splat, heat transfer toward the colder substrate, and the rapid solidification of the material. Although observed on a single particle, these fundamental mechanisms play a crucial role in understanding the overall behavior of a thermally sprayed coating.

Such analysis is not merely of theoretical interest; it also holds significant practical importance, as it helps identify the optimal conditions required to enhance the durability and performance of coatings in various industrial sectors. For instance, in the aerospace field, thermal spray coatings are used to protect turbine blades against wear and extreme temperatures; in the biomedical sector, they are applied to implants to improve biocompatibility and corrosion resistance; and in the energy industry, they are employed to extend the service life of components exposed to harsh environments. Consequently, the in-depth investigation of individual droplet impacts, even within a simplified framework, represents an essential step toward the optimization and industrial deployment of this high-value-added coating process.

III.1.2. PHYSICAL MODEL

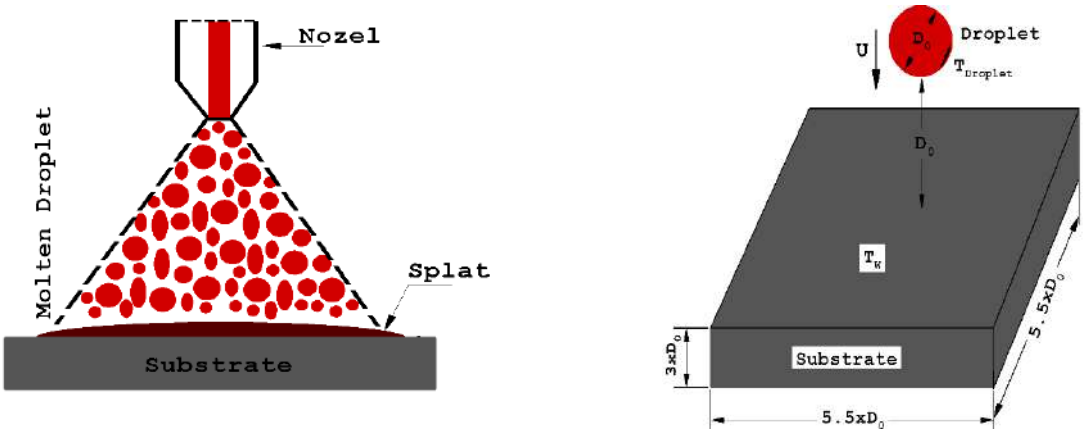


Figure III.1. Thermal **s**pray processes and physical model under analysis**.**

III.1.3. MATHEMATICAL MODEL.

The governing heat transfer equations are solved in ABAQUS/Explicit using an explicit forward-difference time integration scheme [4]. The temperature at a node N for increment $i + 1$ is expressed as:

$$\theta_{(i+1)}^{N} = \theta_{(i)}^{N} + \Delta t_{i+1}\dot{\theta}_{(i)}^{N} \qquad \text{(III.1)}$$

Where $\theta^N$is the nodal temperature and i represents the increment index in a dynamic step. The initial temperature rates are obtained from:

$$\dot{\theta}^N_{(i)} = (C^{NJ})^{-1}(P^J_{(i)} - F^J_i) \quad \text{(III.2)}$$

Here, F^J is the internal flux vector, C^{NJ} is the lumped capacitance matrix, and P^J denotes the applied nodal source vector. The capacitance matrix is defined as:

$$[C] = \int_0^V [V]^T \rho \left(\frac{\partial H}{\partial T}\right)^t N dV \quad \text{(III.3)}$$

within the solidification region, the specific heat capacity is expressed as:

$$C_p(T) = \frac{\partial H}{\partial T} - \frac{H_f}{(T_{liq} - T_{sol})} \quad \text{(III.4)}$$

where H_f is the latent heat of fusion, while T_{sol} and T_{liq} are the solidus and liquidus temperatures, respectively.

The motion equations of the body are integrated explicitly using the central-difference method:

$$\dot{\mu}^N_{(i+1)} = \dot{\mu}^N_{\left(i-\frac{1}{2}\right)} + \frac{\Delta t_{i+1} - \Delta t}{2} \ddot{\mu}^N_{(i)} \quad \text{(III.5)}$$

$$\mu^N_{(i+1)} = \mu^N_i + \Delta t_{i+1} \dot{\mu}^N_{\left(i+\frac{1}{2}\right)} \quad \text{(III.6)}$$

Where μ^N is a degree of freedom (displacement or rotation), the central-difference operator updates the kinematic state explicitly using known velocity and acceleration values from the preceding increment.

The material response is assumed to be linearly elastic, described by the **Mie–Grüneisen Equation of State**. In ABAQUS, pressure is expressed as:

$$P - P_H = \Gamma_\rho (E_m - E_H) \quad \text{(III.7)}$$

With Γ_ρ representing the Grüneisen ratio, and P_H and E_H being Hugoniot pressure and energy, which depend on density. The ratio is defined as:

$$\Gamma = \Gamma_0 \frac{\rho_0}{\rho} \quad \text{(III.8)}$$

Where Γ_0 and ρ_0 are material constants. Hugoniot energy is given by:

$$E_H = \frac{P_H \eta}{2\rho_0} \quad \text{(III.9)}$$

with $\eta = 1 - \frac{\rho_0}{\rho}$ representing nominal compressive strain. Substituting into previous relations yields:

$$P = P_H\left(1 - \frac{\Gamma_0\eta}{2}\right) + \Gamma_0\rho_0 \mathrm{E}_m \quad \text{(III.10)}$$

Hugoniot data are typically fitted using:

$$P_H = \frac{\rho_0 c_0^2 \eta}{(1-s\eta)^2} \quad \text{(III.11)}$$

Where c_0 and s describe the linear relation between shock velocity U_s and particle velocity U_p:

$$U_S = c_0 + sU_P \quad \text{(III.12)}$$

Hence, the Hugoniot form becomes:

$$P = \frac{\rho_0 c_0^2 \eta}{(1-s\eta)^2}\left(1 - \frac{\Gamma_0\eta}{2}\right) + \Gamma_0\rho_0 E_m \quad \text{(III.13)}$$

At minor compressive strains, the bulk modulus reduces to $\rho_0 c_0^2$.

Viscosity evolution is described by the **Arrhenius relationship** [26]:

$$\mu(T) = \mu_0 exp\left(\frac{E}{RT}\right) \quad \text{(III.14)}$$

Where μ_0 is the pre-exponential factor, E the activation energy for viscous flow, T the absolute temperature, and R the universal gas constant ($8.3144\ J * mol^{-1} * K^{-1}$).

III.2. NUMERICAL SIMULATION

III.2.1. INTRODUCTION

In this study, due to the occurrence of significant mechanical deformations combined with simultaneous heat transfer, it was deemed necessary to adopt a coupled temperature–displacement dynamic approach. This strategy makes it possible to realistically capture the interaction between mechanical phenomena (such as plasticity and deformation) and thermal phenomena (such as conduction and heat dissipation), which occur simultaneously during the impact of a molten particle on a metallic substrate.

To achieve a suitable geometric discretization, a tetrahedral mesh was generated to the boundary surfaces whenever regularity and accuracy of the geometry required it. The choice of the **C3D10MT** element proved particularly relevant: it is a second-order, 10-node tetrahedral element, thermally modified and equipped with hourglass control. This element type is widely recognized as well-suited for complex thermo-mechanical analyses, as it enables a more accurate representation of temperature and deformation gradients in highly loaded three-dimensional configurations. Furthermore, to enhance the robustness of the simulation and

mitigate the occurrence of numerical instabilities, a quadratic bulk viscosity was introduced. This feature contributes to damping out artificial oscillations that can arise under rapid dynamic conditions such as those observed during impact.

To model the physical interactions at the particle–substrate interface, a surface-to-surface contact algorithm was employed. This choice allows for a more realistic representation of stress and heat transfer at the impact zone, while preventing non-physical penetrations between the meshes of the two solids. Within this framework, the coefficient of friction was assumed constant and temperature-independent—an assumption that, while simplifying, is commonly adopted to reduce model complexity while still yielding results representative of the overall behavior.

In the configuration under investigation, an aluminum particle was modeled impacting three different metallic substrates: nickel, stainless steel, and copper. The use of the explicit integration method **Abaqus/Explicit** is justified by its ability to efficiently handle fast transient phenomena, large deformations, and complex contact conditions, all of which are characteristic of this type of simulation. The particle was initialized at a temperature of **660 °C**, corresponding to its molten state, and an impact velocity of **150 m/s**, reflecting the typical kinematics of thermal spray processes. The substrate temperature ranged between **20 °C** and **100 °C**, which represents industrial conditions where substrates are generally not preheated to high temperatures, although slight prior heating may occur.

This modeling approach therefore provides deeper insights in to the thermo-mechanical behavior of a particle upon impact on different materials. It yields valuable information regarding spreading, heat dissipation, and stress generation parameters that are key to optimizing adhesion and the overall quality of coatings produced by thermal spraying.

III.2.2. GRID MESH.

As shown in Figure.III.2, the mesh density has an apparent effect on the accuracy of the results. Simulations conducted with a coarse mesh (5724nodes) exhibit larger deviations and scattered trends, whereas the semi-fine mesh (11,449 nodes) yields predictions closer to experimental data. The fine mesh

(17,172 nodes) achieves the best agreement, with minimal error. Consequently, all subsequent numerical

simulations in this study adopt the fine mesh configuration to ensure higher accuracy.

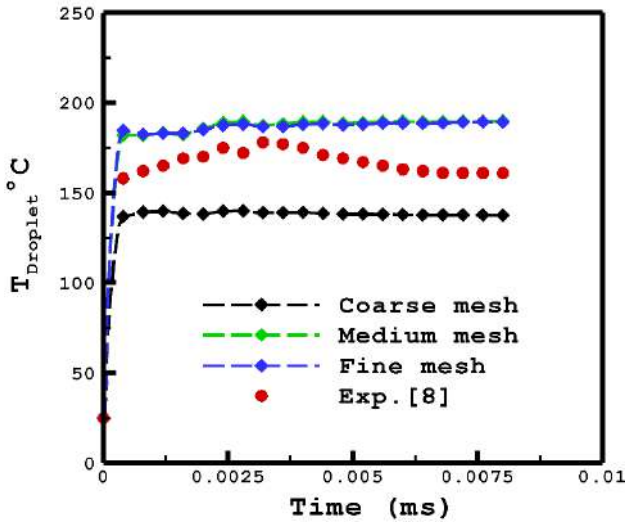


Figure III.1. Magnetisation Grid of Sensitivity of Mesh.

This study begins with an analysis of the normal impact of a molten tin droplet on a flat stainless-steel substrate. This methodological choice is deliberate, as it builds upon previous research, notably the work of Passandideh-Fard et al. [3], who highlighted the fundamental characteristics of this type of interaction through experimental investigations, as well as that of Subedi et al. [2], who provided complementary insights using numerical simulations based on the Smoothed Particle Hydrodynamics (SPH) method. The objective here is to confront new experimental observations with these reference results in order to validate the consistency of the observed behaviors and to gain a deeper understanding of the underlying mechanisms.

Figure III.3 illustrates the results obtained in the framework of our own experiments, conducted under two distinct thermal regimes of the substrate: a wall temperature of 25 °C, representative of near-ambient conditions, and a temperature of 150 °C, corresponding to a significantly higher thermal state. In both cases, the droplet, with an average diameter of 2.1 mm, was propelled toward the surface at an impact velocity of 1.6 m/s, to ensuring consistent comparison of the outcomes between the two configurations.

A key parameter of the study lies in the control of the droplet's initial temperature, which was set at 240 °C. This value, slightly above the melting point of tin (232 °C), guarantees that the droplet remains fully in the liquid state during its flight, thereby eliminating the effects of premature solidification. This methodological choice is consistent with both previous experimental observations and available numerical simulations, thereby reinforcing the credibility and robustness of the results obtained.

In summary, this first experimental stage aims to establish a solid foundation for the analysis by directly comparing the impact and spreading dynamics of the droplet under contrasting thermal conditions. It makes it possible to identify potential differences related to wall temperature while consolidating the scientific validity of the adopted approach. This comparative and confirmatory process constitutes an essential prerequisite before extending the analysis to more complex conditions involving different materials or broader temperature ranges.

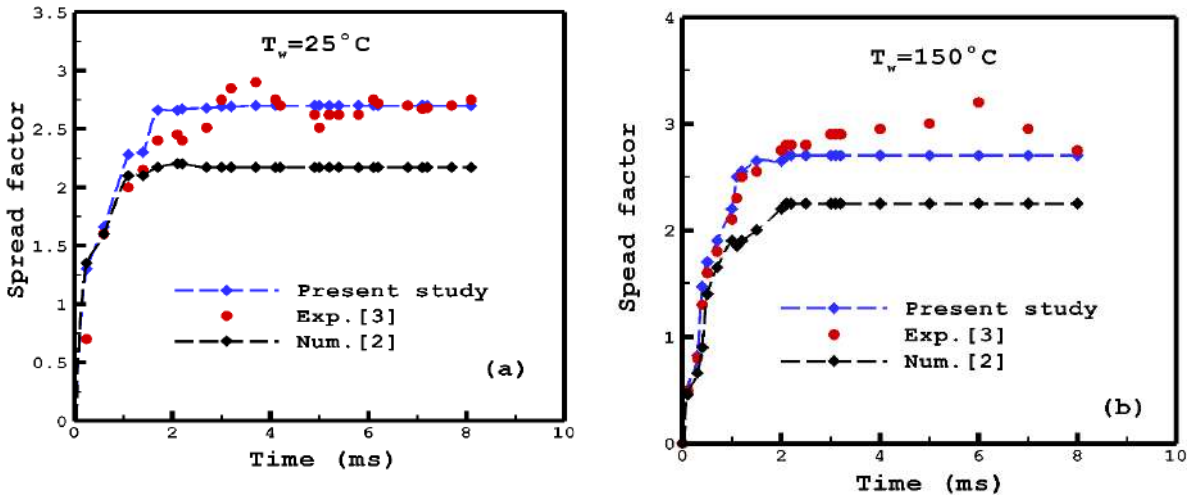


Figure III.3. A tin droplet's spread factor changes at (a) Tw=25°C and (b) Tw=150°C on a stainless steel substrate.

As illustrated in Figure 4, the study focuses on examining the influence of two distinct wall temperature regimes, namely 25 °C and 150 °C, on the behavior of a molten tin droplet impacting a stainless-steel substrate. In each experimental condition, a droplet with a diameter of 2.1 mm and an impact velocity of 1.6 m/s was employed to ensure consistent and comparable scenarios. The initial droplet temperature was set to 240 °C, slightly above its melting point of 232 °C. This choice was based on converging results from both experimental investigations and numerical simulations, thereby ensuring the validity of the observations.

The evolution of the spread factor is accurately reproduced, clearly revealing a trend that is consistent with numerical predictions. Although both experimental data and simulations carry their own intrinsic limitations, the overall agreement between the two approaches adds significant robustness to the analysis. In both thermal configurations, the spreading dynamics of the droplet were recorded precisely up to approximately 2 ms after impact, during which the rapid spreading reflects the dominance of initial inertial effects.

Beyond this timescale, as the droplet begins to solidify, slight discrepancies emerge between numerical predictions and experimental measurements. These differences highlight the complexity of the solidification process and the associated heat transfer mechanisms at the droplet–substrate interface. They are particularly expressed by the progressive stabilization of the spread factor, which tends toward a constant value. This behavior indicates that, once solidified, the droplet no longer undergoes significant morphological changes.

Within this framework, the study incorporates a numerical model based on the mushy zone approach. This solidification model assumes that, during the transition from liquid to solid, the frozen particles are assigned infinite viscosity, which prevents further spreading, and zero velocity, which corresponds to the complete cessation of flow. Although idealized, this representation effectively captures the transition between liquid and solid regimes and provides a reliable approximation of the droplet's overall behavior during impact and solidification.

Thus, this analysis not only highlights the effect of substrate thermal conditions on impact dynamics but also underscores the importance of carefully coupling experimental and modeling approaches to better understand the complex transient phenomena associated with the rapid spreading and solidification of molten materials.

This property effectively halts any further spreading of the droplet, marking the transition from a dynamic liquid state to a quasi-solidified form. It is important to note that tin, when in its molten state, exhibits a high affinity for oxidation upon exposure to air. During the droplet's flight toward the substrate, the rapid cooling and substantial deformation induce the formation of thin oxide layers on its surface. These oxide layers play a critical role in modifying the droplet's wetting behavior and adhesion characteristics, influencing both the final spread factor and the microstructure of the solidified material.

In order to investigate the effect of substrate characteristics on droplet behavior, a polished stainless-steel specimen was employed in this study. The choice of a polished surface allows for controlled observation of the interactions between droplet and substrate while minimizing uncontrolled surface features. Nevertheless, it is recognized that surface roughness can exert a dual influence: on one hand, it tends to slow down solidification and reduce the rate of heat transfer due to localized thermal barriers; on the other hand, increased roughness introduces mechanical resistance that hinders the lateral spreading of the droplet. These competing effects highlight the complexity of accurately modeling droplet–substrate interactions in real-world conditions.

Consequently, the present numerical and analytical models explicitly incorporate surface roughness as a critical parameter. By accounting for the microscale topography of the

substrate, the models are able to more faithfully represent the dynamics of droplet spreading, solidification, and eventual arrest. This approach provides a more comprehensive understanding of how substrate properties interact with fluid behavior and thermal phenomena, ensuring that the predictions align more closely with experimental observations. Incorporating these effects is especially significant when considering applications where precise control of coating thickness, morphology, and adhesion is required, such as in thermal spraying, microfabrication, and surface engineering processes.

Ultimately, the integration of oxidation effects, rapid solidification, deformation, and surface roughness into the modeling framework offers a more realistic and nuanced depiction of the droplet impact phenomenon, bridging the gap between idealized assumptions and practical experimental conditions. This holistic approach enhances both the predictive accuracy of simulations and the interpretive value of experimental results, laying a robust foundation for subsequent investigations into molten metal deposition processes

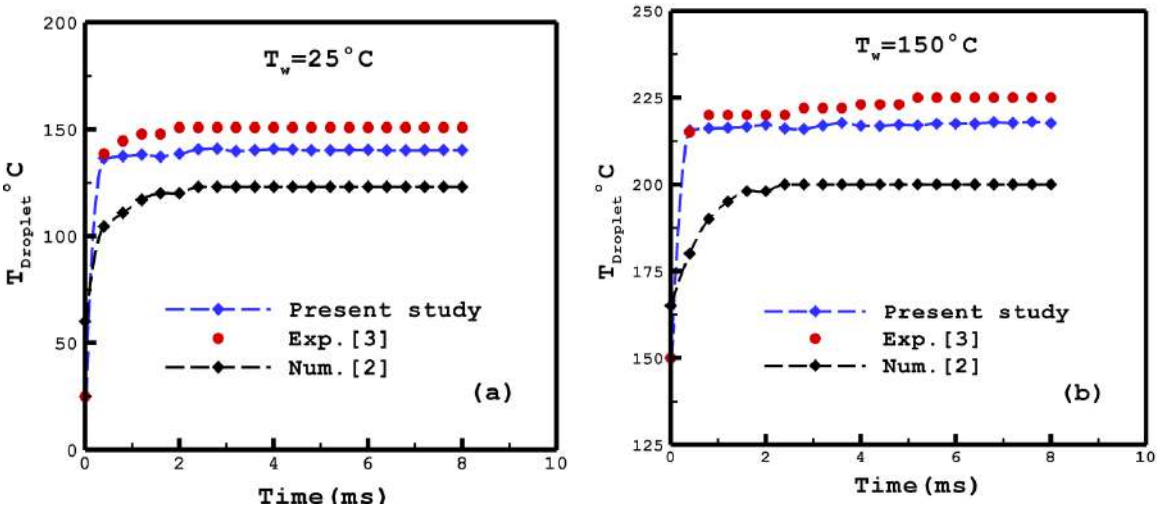


Figure III.4. Temperature evolution at the impact point of a tin droplet on a stainless-steel substrate at two initial wall temperatures: (a) Tw = 25 °C and (b) Tw = 150 °C.

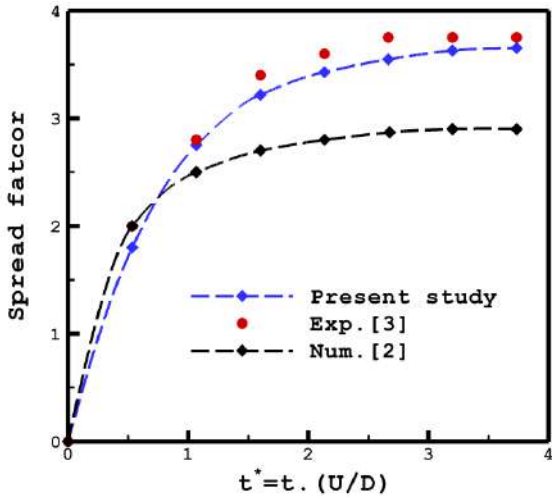


Figure III.5. Evolution of the spread factor for a tin droplet impacting an aluminum substrate (substrate temperature Tw = 26 °C, droplet temperature TD = 267 °C, droplet diameter D = 3.7 mm, and impact velocity U = 2.48 m/s).

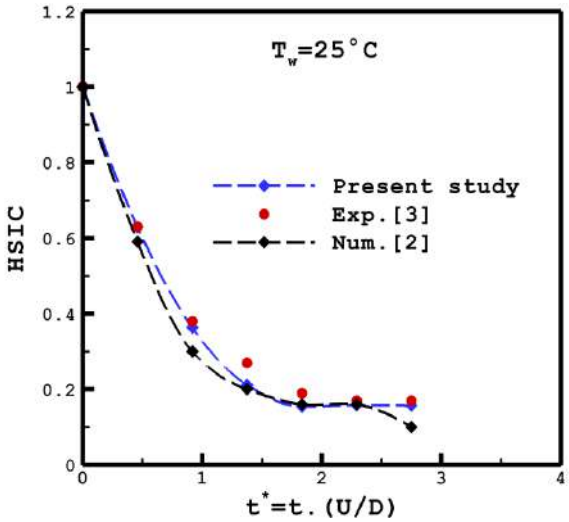


Figure III.6. Evolution of the dimensionless central splat height for the high-speed impact and contact (HSIC) of a copper droplet on a copper substrate. The simulation parameters are: droplet temperature (T_d= 1531 K), substrate temperature (T_w= 295 K), impact velocity (U = 2.52 m·s^{-1}), and droplet diameter (D = 4.67 mm).

The numerical model successfully captured the rapid rise in substrate temperature at the center of impact, reflecting the intense thermal interaction between the molten droplet and the substrate immediately after contact. Experimental results indicate that following this initial surge, the substrate temperature stabilizes relatively quickly. In contrast, the present simulations exhibit a more gradual increase toward a steady-state temperature, highlighting the model's sensitivity to heat conduction and transient energy distribution within the substrate. This behavior emphasizes the importance of accurately modeling the coupled thermal dynamics, as

even slight deviations in heat transfer assumptions can significantly influence the predicted thermal history of both the droplet and the substrate.

To validate the robustness of the model, its predictions were compared with the experimental findings of Trapaga et al. [6], which included measurements of the dimensionless splat height of copper (Cu) droplets impacting a copper substrate and the dimensionless spread factor of tin (Sn) droplets impacting an aluminum (Al) substrate. These comparisons provide a benchmark for assessing the model's ability to account for variations in substrate material, droplet composition, and impact conditions, thereby offering a more comprehensive evaluation of droplet–substrate interactions across different metallurgical systems.

The simulations included two representative cases. In the first, a tin droplet with a diameter of 3.7 mm and an initial temperature of 267 °C impacted an aluminum substrate maintained at 26 °C. The droplet approached vertically with a velocity of 2.48 $m \cdot s^{-1}$, providing a controlled scenario to study spreading dynamics, thermal conduction, and solidification on a relatively low-melting-point substrate. In a second, more extreme case involving copper on copper, the model simulated a molten droplet starting at 1252 °C, with a diameter of 4.67 mm and a vertical impact velocity of 2.52 $m \cdot s^{-1}$, striking a substrate maintained at 22 °C. Figures 5 and 6 illustrate these scenarios, showing a strong agreement between the predicted spread factors and experimental measurements, largely attributable to the model's incorporation of thermal conductivity and phase change effects.

The model also provides insight into secondary phenomena associated with thermal spraying, including droplet melting, re-solidification, and transient temperature distribution within both droplet and substrate. By capturing these coupled processes, the simulation framework allows for a detailed exploration of the temporal evolution of droplet morphology, the development of thermal gradients, and the resulting microstructural characteristics. These capabilities are particularly relevant for applications in coating technologies, additive manufacturing, and surface engineering, where precise control of droplet behavior and thermal histories is critical to ensuring the quality, adhesion, and functional properties of the deposited material.

In summary, the extended modeling approach not only reproduces the experimentally observed spread factors with high fidelity but also provides a predictive tool for investigating the complex interplay between droplet material, substrate properties, and impact conditions. This establishes a solid foundation for subsequent analyses of thermal spray processes and supports the design of optimized deposition strategies for advanced material systems.

Chapter IV RESULTS AND DISCUSSION

IV.1. INTRODUCTION

To achieve a deeper understanding of the droplet solidification phenomenon within the thermal spraying process, two complementary case studies were designed and executed. The first case focused on the behavior of a single droplet, allowing for a controlled and detailed analysis of its thermal, mechanical, and phase-change dynamics during impact and subsequent solidification. By isolating a single particle, the study was able to capture critical features such as the rate of heat transfer between droplet and substrate, the evolution of the droplet's morphology, the formation of oxide layers, and the onset of solidification in relation to both droplet temperature and substrate conditions. This approach provides a fundamental baseline for understanding the intrinsic mechanisms governing droplet-substrate interactions and the transition from a molten to a solid state.

The second case extended the investigation to a multiparticle configuration, which more closely mimics real industrial thermal spraying conditions. In this scenario, interactions between droplets, as well as cumulative effects on the substrate temperature and surface morphology, were carefully examined. The presence of multiple droplets introduces additional complexities, including overlapping splats, variations in local cooling rates, and potential remelting of previously deposited material. These phenomena have significant implications for the microstructure, adhesion, and uniformity of the final coating, as well as for the evolution of residual stresses and porosity within the deposited layer.

Together, the single- and multiparticle studies provide a comprehensive perspective on the thermal spraying process, bridging the gap between fundamental droplet-scale mechanisms and practical, large-scale deposition behavior. By combining these two approaches, the analysis not only elucidates the kinetics of droplet solidification but also enables the development of predictive models that account for both individual particle dynamics and collective effects in multilayer coatings. This dual approach is essential for optimizing process parameters, improving coating quality, and advancing the scientific understanding of thermal spray deposition mechanisms.

Finally, we sought to answer the following question: what is the influence of particle (projected droplet) shape on the thermal behavior during impact on the substrate? To this end,

we simulated the impact of an aluminum droplet with an elliptical geometry on a stainless steel substrate. The temporal evolution of the substrate temperature, the deformed droplet temperature, and the thickness of the solidified layer was monitored and quantified, and then systematically compared with that obtained for a droplet of spherical geometry.

This parametric analysis provides deeper insight into the role of particle morphology in heat transfer and solidification mechanisms, which is a key issue for the optimization of thermal spraying processes. The results show that the elliptical particle exhibits more efficient thermal diffusion than the spherical one, suggesting that accounting for the actual droplet geometry can improve the accuracy of predictive models and contribute to better control of the final coating properties.

IV.2. FIRST SECTION, A SINGLE PARTICLE

The numerical model developed in this study provides a detailed simulation of the impact and spreading of a single aluminum particle on a steel substrate within the context of thermal spraying. The model employs an explicit dynamic formulation that couples both temperature and displacement fields, allowing for the simultaneous capture of thermal conduction, phase change, and mechanical deformation during the droplet–substrate interaction. This approach enables a comprehensive representation of the transient phenomena that occur during particle impact, including rapid flattening, heat transfer to the substrate, and the onset of solidification.

IV.2.1. STAINLESS-STEEL SUBSTRATE

Our results provide a comprehensive prediction of the thermal evolution of a 2.1 mm diameter Aluminum droplet impacting a stainless-steel substrate under two distinct thermal conditions: 25 °C and 150 °C. The droplet, entering the system with an initial velocity of 1.6 m/s and a temperature of 240 °C (slightly above its melting point) undergoes rapid spreading immediately upon impact, followed by progressive solidification. The evolution of this process is governed by a complex interplay between inertial forces, thermal conduction, and phase-change phenomena, which collectively dictate the droplet's deformation and solidification behavior.

As illustrated in Figure IV.1 and IV.2, the substrate's initial temperature exerts a significant influence on the cooling rate of the droplet, which in turn affects the kinetics of solidification and the resulting microstructure of the deposited material. A higher substrate temperature slows the dissipation of thermal energy from the droplet, thereby prolonging the liquid state and promoting more extensive spreading, whereas a lower substrate temperature

accelerates cooling and reduces the extent of droplet deformation. Figure 9, showing the droplet contours at various time intervals, provides additional visual confirmation of these phenomena, highlighting differences in spread morphology and solidification progression between the two thermal conditions.

The onset of solidification is observable immediately upon contact with the substrate. This process is initiated by the rapid transfer of thermal energy from the molten droplet to the comparatively cooler substrate, leading to a phase transition from liquid to a mushy state, and eventually to solid. During this transformation, the droplet simultaneously dissipates both kinetic and thermal energy, which contributes to the formation of a well-defined splat structure. The dynamic nature of this phase transition underscores the importance of considering coupled thermal and mechanical effects in modeling droplet impact phenomena.

Furthermore, these results emphasize that substrate temperature is not merely a boundary condition but a critical parameter that directly affects droplet morphology, spreading dynamics, and solidification patterns. Understanding this relationship provides valuable insight into optimizing process parameters in thermal spraying, particularly for controlling coating thickness, microstructural homogeneity, and adhesion strength. Such detailed characterization of droplet–substrate interactions lays a foundation for predictive modeling of multiparticle deposition and more complex industrial thermal spray processes.

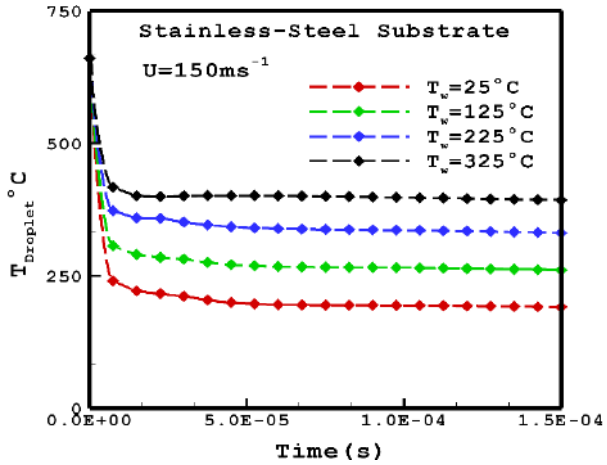


Figure IV.1. Thermal response of an aluminum droplet impacting a stainless-steel substrate at varying wall temperatures ($U = 150\ ms^{-1}$).

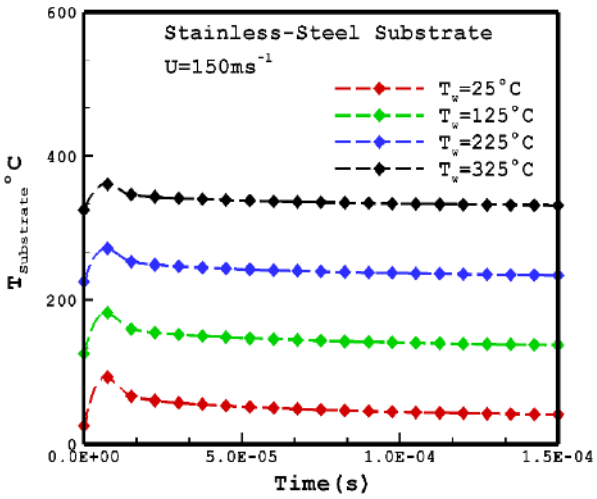


Figure IV.2. Transient temperature evolution at the impact point of a stainless-steel substrate by an Aluminum droplet at various initial substrate temperatures ($U = 150\ ms^{-1}$).

The figure IV.3 illustrates the thermal evolution of a droplet impacting a stainless steel substrate at 100 m·s⁻¹ for different substrate temperatures. A rapid temperature drop is observed immediately after impact, as a direct consequence of the steep thermal gradient and the intense heat transfer at the interface.

The transient phase is followed by a quasi-steady regime, whose value depends strictly on the initial substrate temperature: the hotter the substrate, the higher the droplet's equilibrium temperature. This trend reflects a reduction in the heat extraction exerted by the substrate as its temperature increases.

These results confirm the decisive role of substrate temperature in the cooling and solidification kinetics of droplets, and consequently in the quality and density of the coating obtained by thermal spraying.

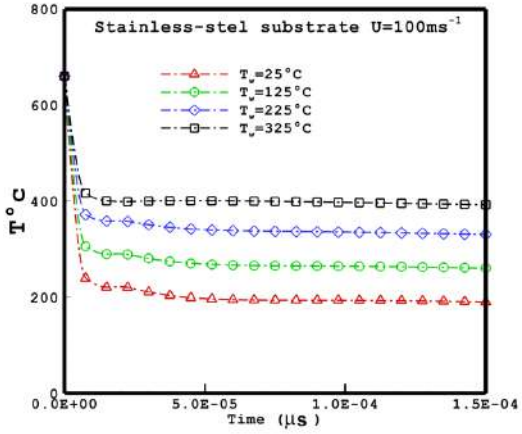


Figure IV.3. Transient Thermal Behavior of an Aluminum Droplet Impacting stainless-steel substrates at Different Initial Temperatures (U = 100 m·s⁻¹)

According to the figure IV.4, the substrate temperature undergoes a transient variation during the droplet impact. A significant temperature rise is observed immediately upon contact, as a direct consequence of the intense heat transfer at the droplet–substrate interface. This transient phase is followed by a rapid stabilization of the temperature after a very short duration. The magnitude of this variation is strongly influenced by the initial preheating temperature of the substrate: the higher the preheating temperature, the greater the observed temperature increase. These results highlight the critical role of substrate preheating in the thermal transfer kinetics and, consequently, in the overall thermal behavior of the substrate during impact.

In addition, the temporal evolution of the temperature suggests that the heat exchange is initially dominated by conduction within a very thin region close to the interface, before progressively diffusing into the bulk of the substrate. This behavior indicates that the characteristic timescale of the thermal response is much shorter than the hydrodynamic timescale associated with droplet spreading and recoil. As the substrate temperature approaches a quasi-steady value, the heat flux at the interface decreases, reflecting a reduction in the temperature gradient between the droplet and the solid surface. Furthermore, for higher preheating temperatures, not only is the peak temperature more pronounced, but the substrate also takes longer to dissipate the absorbed energy into its interior, pointing to a stronger thermal loading.

Such observations are of particular importance for applications involving rapid droplet deposition or thermal spraying, where the substrate temperature directly affects wetting, solidification, and adhesion phenomena. A properly controlled preheating strategy can therefore be used to tailor the interfacial temperature history, optimize the heat transfer rate, and improve the final quality of the deposited layer. Overall, the analysis of the temperature evolution during impact confirms that substrate preheating is a key parameter governing both the intensity and the dynamics of thermal exchanges in droplet–surface interactions.

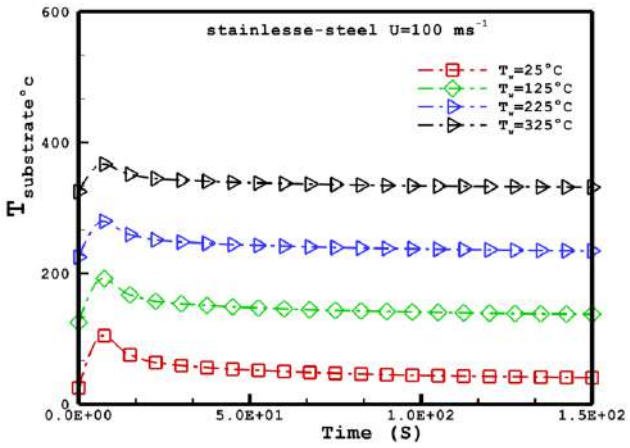


Figure IV.4. Time-Dependent Temperature Evolution at the Impact Site of a Stainless-Steel Substrate Subjected to Aluminum Droplet Deposition (U = 100 $m \cdot s^{-1}$)

IV.2.2. COPPER SUBSTRATE

The figures IV.5 and IV.6 illustrate the thermal evolution of an aluminum droplet impacting a copper substrate at velocities of 100 $m \cdot s^{-1}$ and 150 $m \cdot s^{-1}$, for various initial substrate temperatures. Immediately after impact, a rapid temperature drop is observed, resulting directly from the steep thermal gradient and the intense heat transfer at the interface. This transient phase is followed by a quasi-steady regime, whose value is closely correlated with the initial substrate temperature: the higher the substrate temperature, the higher the droplet's equilibrium temperature, reflecting a reduction in the heat extraction exerted by the substrate.

These observations highlight the critical role of substrate temperature in the cooling and solidification kinetics of droplets, and, consequently, in the quality and density of the coating produced by thermal spraying. Furthermore, the droplet velocity significantly influences the heat exchange with the substrate. Indeed, an increase in velocity leads to a lower droplet temperature at impact, as a result of more rapid deformation and an increased contact surface between the droplet and the substrate.

In addition, the combined effects of impact velocity and substrate preheating condition the characteristic timescales of solidification. At higher impact velocities, the enhanced spreading promotes more efficient heat transfer, thereby accelerating the cooling process and potentially leading to finer microstructures in the solidified splat. Conversely, for lower impact velocities or insufficient substrate preheating, the reduced interfacial heat flux may induce

incomplete spreading, premature solidification at the periphery, and the formation of defects such as porosity or weakly bonded regions.

The numerical results also suggest that the thermal response of the droplet is highly sensitive to the initial temperature difference between the aluminum and the copper substrate. When this temperature difference is large, the droplet experiences a sharp initial cooling rate, which can favor rapid nucleation and the development of high residual thermal stresses within the coating. On the other hand, when the substrate is preheated to higher temperatures, the decrease in the driving thermal gradient moderates the cooling rate, thereby promoting improved metallurgical bonding and reducing the likelihood of cracking or delamination.

Overall, the analysis of figures IV.5 and IV.6 confirms that both the substrate temperature and droplet impact velocity are key operating parameters that must be carefully adjusted to control the thermal history of the droplet, the solidification dynamics, and ultimately the microstructural and mechanical properties of the deposited coating in thermal spraying processes.

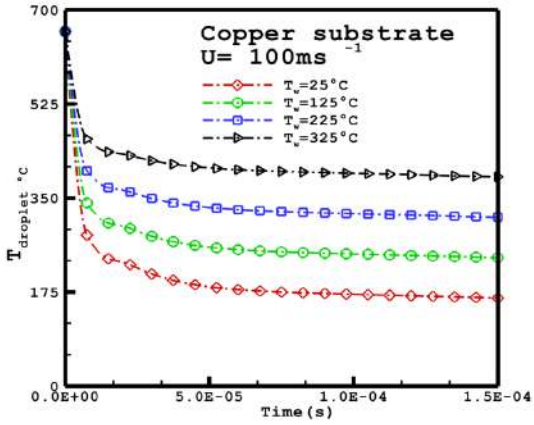


Figure IV.5. Transient Temperature Dynamics of an Aluminum Droplet Impacting Copper Substrates under Varying Preheating Conditions (U = 100 m·s⁻¹)

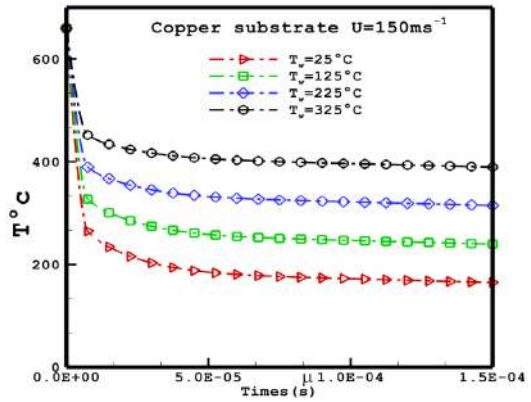


Figure IV.6. Transient Temperature Dynamics of an Aluminum Droplet Impacting Copper Substrates under Varying Preheating Conditions (U = 100 m·s⁻¹)

According to Figures IV.7 and IV.8, the substrate temperature undergoes a pronounced transient variation during droplet impact. A significant temperature rise is observed immediately upon contact, resulting directly from the steep thermal gradient and the intense heat transfer at the droplet–substrate interface. This transient phase is short-lived and is rapidly followed by stabilization toward a quasi-steady state, reflecting the balance between the thermal input from the droplet and the substrate's heat capacity.

The magnitude of this variation is strongly dependent on the initial preheating temperature of the substrate: a higher preheated substrate induces a greater local temperature increase due to the reduced heat extraction by the substrate. These observations confirm the critical role of substrate preheating in the thermal transfer kinetics, droplet solidification, and, consequently, in the quality and density of the coating produced. Furthermore, the droplet impact velocity is a key parameter influencing heat transfer. An increase in impact velocity results in greater droplet deformation and an enlarged contact area with the substrate, enhancing the instantaneous heat flux. However, when the substrate temperature approaches the melting point of aluminum, the effect of impact velocity diminishes, as the temperature difference between the droplet and the substrate decreases, limiting the thermal gradient at the interface. These results highlight the complex interplay between substrate preheating and droplet impact velocity in determining the local thermal profile during thermal spray deposition.

In addition, the temporal evolution of the substrate temperature suggests that heat transfer is initially governed by highly localized conduction in a thin region beneath the impact zone, before progressively diffusing into the bulk of the material. This behavior indicates that the characteristic thermal response time of the substrate is significantly shorter than the hydrodynamic timescale associated with droplet spreading and recoil. As the temperature distribution becomes more uniform, the interfacial heat flux progressively decreases, illustrating the attenuation of the driving thermal gradient. This mechanism is particularly marked for highly preheated substrates, where the relatively small temperature difference between the droplet and the solid limits the net heat extraction, thereby promoting a higher local temperature plateau.

Moreover, the combined effect of substrate preheating and impact velocity conditions the solidification front dynamics within the droplet. For moderate substrate temperatures and high impact velocities, the intense and rapid heat extraction can induce a steep solidification front, leading to refined microstructures and potentially higher hardness in the resulting splat. Conversely, in the case of elevated substrate temperatures, the reduced cooling rate may favor the development of coarser microstructures, improved wetting, and enhanced metallurgical

bonding at the interface. This trade-off between cooling intensity and bonding quality underscores the need to adjust process parameters according to the desired coating properties.

From a process engineering perspective, the numerical trends observed in Figures IV.7 and IV.8 underline that substrate preheating cannot be considered independently of impact velocity. At low substrate temperatures, the influence of velocity on the thermal response is predominant, since the strong thermal gradient allows significant modulation of the heat flux by changing the contact conditions. In contrast, at high substrate temperatures, the system tends toward a thermally saturated regime in which the velocity mainly affects the geometrical characteristics of the splat (spreading diameter, thickness) rather than the net amount of heat transferred. This regime transition is critical for optimizing thermal spray conditions, as it governs not only the local temperature history but also the formation of residual stresses, porosity, and interfacial defects within the coating.

Overall, the analysis of the substrate temperature evolution confirms that the interplay between substrate preheating and impact velocity constitutes a central lever for controlling the thermal history during deposition. Proper tuning of these parameters enables the tailoring of solidification kinetics, microstructural development, and ultimately the mechanical performance and durability of thermally sprayed coatings.

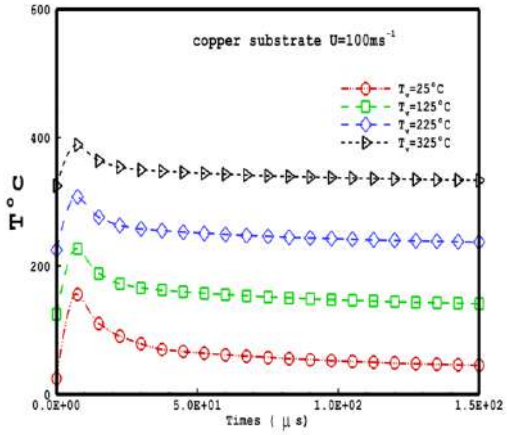


Figure IV.7. Time-Dependent Temperature Evolution at the Impact Site of a cooper Substrate Subjected to Aluminum Droplet Deposition (U = 100 m·s⁻¹)

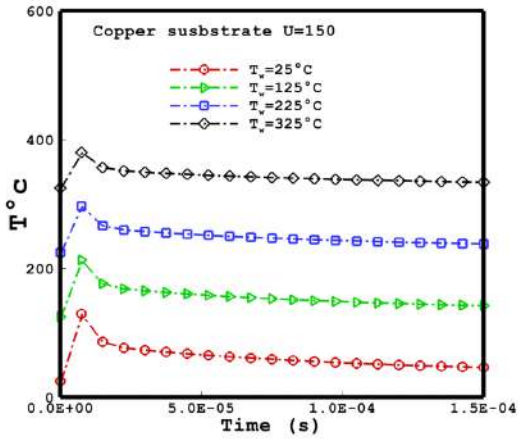


Figure IV.8. Time-Dependent Temperature Evolution at the Impact Site of a cooper Substrate Subjected to Aluminum Droplet Deposition (U = 150 m·s^{-1})

The two graphs (Figure IV.9 and Figure IV.10) depict the temporal evolution of the thickness of a deposited layer on a copper substrate for four substrate temperatures (25 °C, 125 °C, 225 °C, and 325 °C) and two different flow or impact velocities, U=100m\s and U=150 m\s ; in both cases, the abscissa represents time in seconds, the ordinate represents the coating thickness, and the curves display an initially rapid increase followed by a progressive approach to a quasi-steady plateau, indicating the establishment of a stationary deposition regime in which the growth rate tends toward zero. For each velocity, the curves corresponding to the different substrate temperatures are almost superimposed, which shows that, within the investigated temperature range, the substrate temperature exerts only a negligible influence on both the final thickness and the overall growth kinetics of the layer. A comparison of the plateau values reveals, however, that the stationary thickness obtained at U=150m/s is slightly higher than that observed at U=100m\s, suggesting that the impact or flow velocity is a more influential control parameter than the substrate temperature for the amount of material deposited, even though the qualitative shape of the thickness time evolution (transient followed by steady state) remains essentially the same for both operating conditions.

This behavior indicates that, under the present operating conditions, the deposition process is predominantly controlled by the hydrodynamic and inertial characteristics of the incoming droplets rather than by the thermal state of the substrate. The weak sensitivity of the thickness to substrate temperature suggests that, within the range 25 to 325 °C, the modifications in wetting, spreading, and solidification dynamics induced by preheating are not sufficient to significantly alter the net mass accumulation per impact event. Instead, the increase in impact velocity enhances the kinetic energy and deformation of the droplets, promoting more

efficient spreading and potentially reducing rebound or splash phenomena, which in turn results in a slightly higher effective deposition efficiency and a larger asymptotic thickness.

Furthermore, the nearly identical transient durations observed for all substrate temperatures at a given velocity imply that the characteristic timescale associated with the transition from the initial growth phase to the quasi-steady regime is primarily governed by the droplet arrival frequency and impact conditions, rather than by the thermal evolution of the substrate–coating system. The attainment of a plateau in thickness may be interpreted as the result of a balance between the rate of incoming material and possible loss or densification mechanisms (such as splashing, re-melting, or pore closure), leading to an apparent saturation of the layer growth. The slight increase in plateau thickness with higher impact velocity is consistent with an enhanced capture efficiency of the substrate surface, whereby a greater fraction of the impinging droplets contributes effectively to the coating formation.

From a process optimization standpoint, these results underline that adjusting the impact or carrier gas velocity constitutes a more effective means for controlling the final coating thickness than modifying the substrate temperature alone, at least within the moderate preheating range considered. While substrate preheating remains crucial for influencing other aspects of coating quality such as adhesion strength, residual stress distribution, porosity, and microstructural refinement its impact on the macroscopic geometric characteristic of interest here, namely the overall layer thickness, appears secondary compared to the role of velocity. Consequently, the design of operating conditions for thermal spraying should treat impact velocity as a primary control parameter for deposition efficiency, with substrate temperature playing a complementary role mainly through its effects on interfacial bonding and microstructure rather than on net thickness growth.

Overall, the analysis of Figures IV.9 and IV.10 confirms that the coating buildup is governed by a complex but hierarchized coupling between thermal and hydrodynamic parameters, in which the influence of impact velocity on the deposition rate and stationary thickness clearly dominates over that of substrate temperature within the explored parameter space

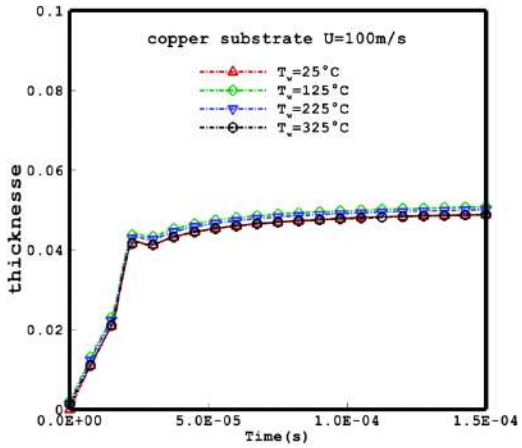


Figure IV.9. Transient Variation of Solidification Thickness of an Aluminum Droplet Impacting a Copper Substrate at 100 $m \cdot s^{-1}$ under Different Substrate Temperatures.

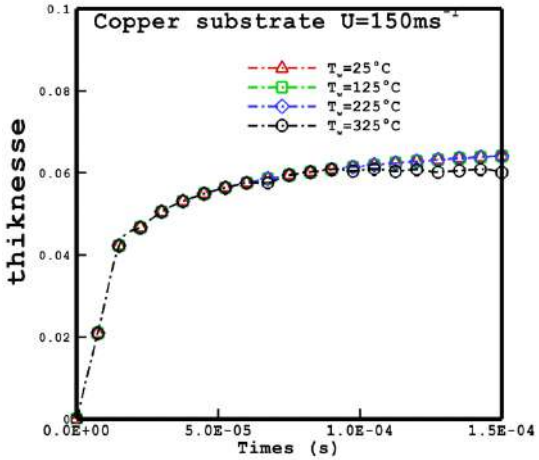


Figure IV.10. Transient Variation of Solidification Thickness of an Aluminum Droplet Impacting a Copper Substrate at 100 $m \cdot s^{-1}$ under Different Substrate Temperatures.

IV.2.3. NICKEL SUBSTRATE

The Figure IV.11 and IV.12 shows that, for all substrate temperatures, the temperature of the deposit drops very rapidly immediately after impact and then gradually stabilizes toward an almost constant plateau. This evolution highlights a transient regime of intense cooling at the very beginning, followed by a phase in which the heat flux decreases as the temperature difference between the droplet and the substrate is reduced. It is also observed that the higher the initial substrate temperature, the higher the corresponding curve remains overall, and the higher the long-term equilibrium temperature. This means that a hot substrate limits the thermal gradient at the interface, slows down the cooling rate of the droplet, and delays the onset of solidification compared with a cold substrate. From a physical point of view, these trends reflect heat transfer dominated by conduction across the deposit–substrate contact zone, where the heat

flux density is directly related to the local temperature difference. A cold substrate induces high quenching rates, promoting the formation of very fine microstructures and high residual stresses, whereas a preheated substrate prolongs the liquid phase, improves wetting, and can lead to more extensively spread and more continuous splats in thermal spray processes.

Beyond this first qualitative analysis, the shape of the curves suggests that the thermal response of the deposit can be interpreted in terms of characteristic timescales associated with heat diffusion within both the droplet and the substrate. The steep initial temperature decrease corresponds to a short conduction timescale, during which heat is rapidly transferred across a thin interfacial region. As time progresses, the thermal gradients progressively relax, and the system approaches a quasi-steady regime controlled by the effective thermal capacities and conductivities of the materials involved. In this regime, additional temperature variations become marginal, indicating that the local thermal equilibrium between the deposit and the substrate has been almost fully established.

Moreover, the systematic upward shift of the curves with increasing substrate temperature indicates that the thermal history of the deposited material is highly sensitive to the initial energy content of the solid support. For a cold substrate, the large initial temperature difference enhances the driving force for heat extraction, which shortens the solidification time and favors rapid nucleation and growth of fine grains. Conversely, when the substrate is preheated to higher temperatures, the reduced thermal gradient moderates the cooling rate, extends the duration of the liquid state, and allows for more extensive spreading and possible coalescence of successive splats. This can improve inter-splat bonding and reduce the prevalence of defects such as interfacial pores or weakly bonded regions.

From a process engineering standpoint, these results emphasize that substrate preheating is not merely a secondary adjustment parameter, but a central lever for controlling the solidification kinetics and the resulting microstructure of thermally sprayed coatings. By appropriately selecting the preheating temperature, it becomes possible to tailor the balance between rapid quenching—favorable to hardness and fine microstructures—and slower cooling, which promotes better adhesion, reduced residual stresses, and enhanced coating continuity. The analysis of Figures IV.11 and IV.12 therefore confirms that the thermal boundary conditions at the interface, dictated primarily by the substrate temperature, play a decisive role in determining both the short-term thermal evolution of the deposit and the final performance of the coating.

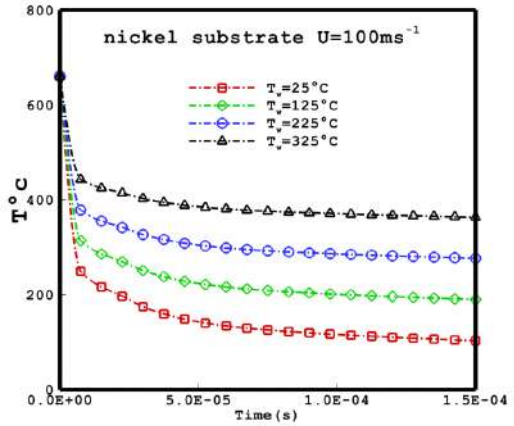


Figure IV.11. Temperature evolution of a droplet of aluminum impacting on nickel substrate at U = 100 m·s⁻¹ for different initial temperatures.

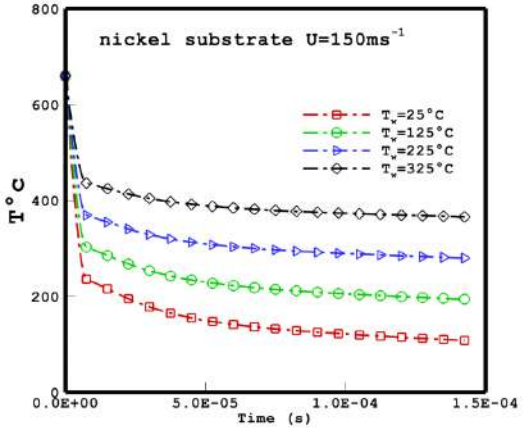


Figure IV.12. Temperature evolution of a droplet of aluminum impacting on nickel substrate at U = 150 m·s⁻¹ for different initial temperatures.

The Figure IV.13 and IV.13 illustrates the thermal response of a nickel substrate subjected to the impact of an aluminum droplet at a velocity of 100 m·s⁻¹, considering several initial substrate temperatures. Immediately after impact, all curves exhibit a sharp rise in temperature, indicating a rapid heat transfer between the hotter droplet and the metallic substrate. This initial increase results from the intense thermal conduction induced by the large local temperature gradient, as well as from the partial conversion of the droplet's kinetic energy into thermal energy at the impact point. The amplitude of this peak decreases significantly as the initial substrate temperature increases: it is highest at 25 °C, where the temperature difference between the droplet and the substrate is greatest, and progressively decreases at 125 °C and 225 °C, reflecting a reduction in the thermal flux. For a substrate initially heated to 325 °C, the peak becomes almost imperceptible, indicating that the temperatures of the two materials are sufficiently close to limit the intensity of the heat exchange. After approximately 5×10^{-5} s, all curves converge toward a quasi-steady regime in which the substrate

temperature varies only slightly. This stage reflects the dominance of heat diffusion mechanisms within the nickel bulk, whose thermal conductivity and heat capacity enable rapid redistribution of energy over a wider region.

Overall, the results highlight the decisive role of the initial thermal gradient in governing the heating dynamics of the substrate. A cold substrate undergoes a more pronounced temperature rise and a more noticeable transient evolution, whereas a hot substrate significantly limits heat transfer and reaches a quasi-equilibrium state more rapidly. These observations are essential for understanding heat-transfer mechanisms in thermal spraying processes, where the substrate's thermal condition directly influences solidification kinetics and the final microstructure of the coating.

Beyond this first level of analysis, the behavior reported in Figure IV.13 reveals that the thermal response of the nickel substrate can be interpreted in terms of transient one-dimensional conduction in a semi-infinite solid subjected to a localized surface thermal load. The very short duration of the initial peak, combined with the rapid attenuation of temperature gradients, suggests a characteristic diffusion timescale compatible with the high thermal diffusivity of nickel. Once this transient is passed, the temperature field tends toward a self-similar profile controlled mainly by the substrate's thermophysical properties, while the influence of the droplet impact conditions becomes secondary.

Furthermore, the progressive attenuation of the peak amplitude with increasing initial substrate temperature clearly underlines the central role of the driving temperature difference at the interface. At low substrate temperatures, the high thermal gradient promotes intense heat fluxes, potentially inducing strong local expansions and, therefore, significant thermomechanical stresses in the near-surface region. Conversely, at elevated preheating temperatures, the weaker gradient leads to a more moderate and spatially diffuse heating, which can limit the development of steep thermal stresses and reduce the risk of crack initiation or interfacial decohesion under cyclic loading.

From a process engineering perspective, these results confirm that controlling the initial substrate temperature makes it possible to tailor the amplitude and duration of thermal shocks generated by successive droplet impacts. In thermal spraying applications, a cold nickel substrate favors rapid heat extraction, strong quenching of the deposited splats, and the formation of refined microstructures, but at the cost of higher residual stresses and a greater susceptibility to defects. In contrast, a preheated substrate attenuates the thermal shock, promotes more gradual heating of the surface layer, and can thus improve adhesion and structural integrity of multilayer coatings, even if the resulting microstructure may be slightly

coarser. Consequently, the choice of substrate temperature must be made by balancing the requirements of mechanical performance, residual stress control, and microstructural refinement in the targeted coating system

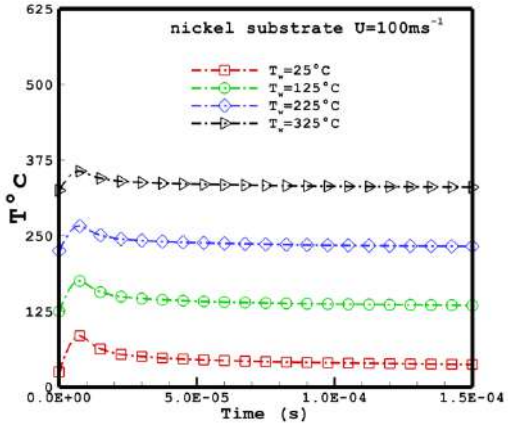


Figure IV.13. Transient Thermal Response of a Nickel Substrate Under Aluminum Droplet Impact (U = 100 m·s⁻¹)

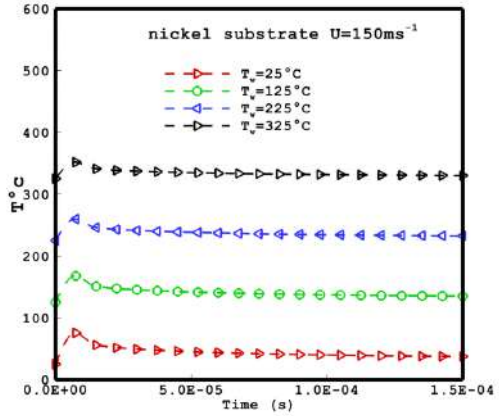


Figure IV.14. Time-Resolved Heating Dynamics of a Copper Substrate Following Aluminum Droplet Impact (U = 150 m·s⁻¹)

The figure IV.15 and VI.16 shows that the solidified thickness of the aluminum droplet increases sharply immediately after impact, reflecting an extremely rapid heat extraction toward the nickel substrate, before approaching a quasi-steady regime once solidification is nearly complete. Increasing the initial temperature of the substrate systematically reduces the final solidified thickness, which indicates a progressive weakening of the thermal gradient imposed at the interface. From a physical standpoint, this behavior highlights the dominant role of transient heat conduction in controlling the solidification kinetics: when the substrate is cold, the large temperature difference between the liquid aluminum and the nickel surface generates an intense heat flux that accelerates nucleation and the propagation of the solid–liquid front. As the substrate is preheated, this gradient decreases, limiting the rate of heat extraction, delaying

the advance of the solidification front, and reducing the extent of the solidified layer. Overall, the observed trends demonstrate that the initial thermal dynamics governed primarily by conductive heat transfer at the moment of impact directly dictate the fraction of the droplet that solidifies and ultimately influence the development of its final microstructure.

The two graphs illustrate the evolution of the solidified thickness of an aluminum droplet impacting a nickel substrate for different substrate temperatures, at two distinct impact velocities: 100 m/s and 150 m/s. In both cases, the solidified layer grows rapidly immediately after impact before approaching a quasi-steady plateau after approximately 1×10^{-4} s, indicating a rapid initial solidification followed by a near-equilibrium regime. For each velocity, the curves consistently show that colder substrates (25 °C) lead to the largest final thickness, whereas hotter substrates (325 °C) result in the smallest, confirming that increasing the substrate temperature reduces the thermal gradient and slows solidification. The gap between the curves corresponding to 25 °C and 325 °C is comparable for both velocities, demonstrating that substrate temperature predominantly governs the solidification kinetics. The effect of impact velocity is also evident: at 150 m/s, the initial increase in thickness is sharper, reflecting more intense initial cooling due to better contact and a larger wetted area, whereas at 100 m/s the rise is slightly less steep. Over longer times, the final plateau thicknesses are similar for both velocities, although slightly higher for colder substrates at 150 m/s, suggesting that a higher impact velocity enhances early-stage solidification without substantially altering the ultimate plateau controlled primarily by substrate temperature. Overall, the graphs indicate that while the general curve shape and the temperature effect are qualitatively identical, increasing impact velocity accentuates the initial solidification phase and slightly elevates early thickness, leaving the long-term solidification outcome largely dictated by the substrate temperature.

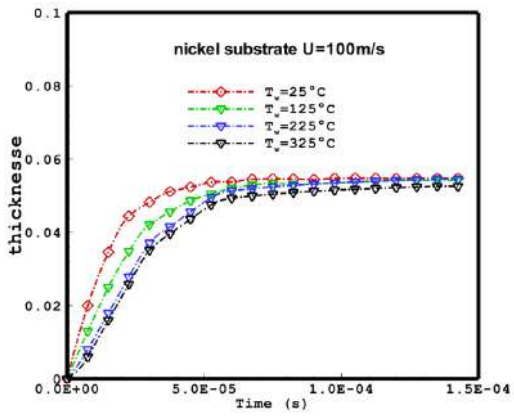


Figure IV.15: Transient Solidification Behavior of an Aluminum Droplet on a Nickel Substrate at 100 $m\cdot s^{-1}$ for Different Initial Substrate Temperatures

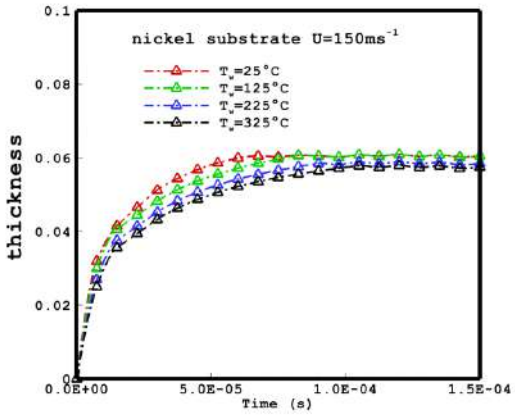
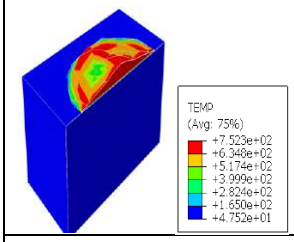
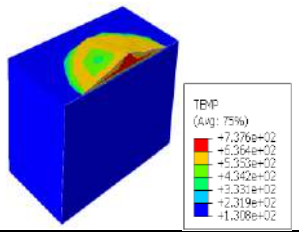
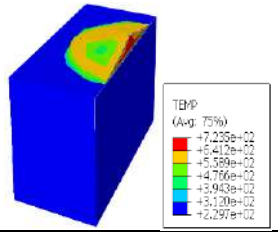
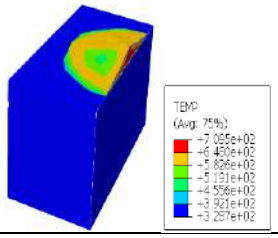
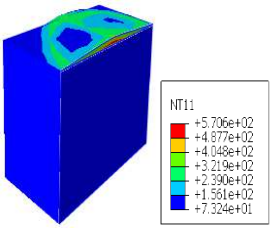
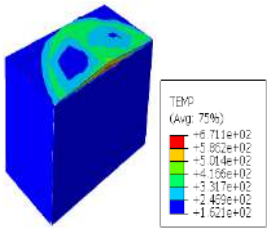
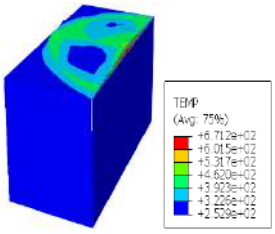
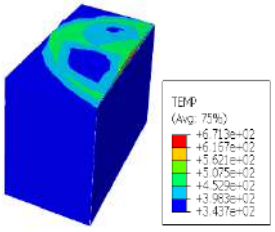
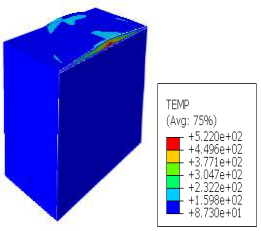
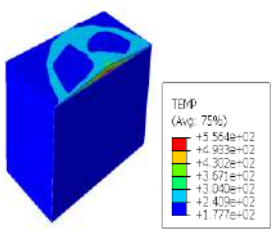
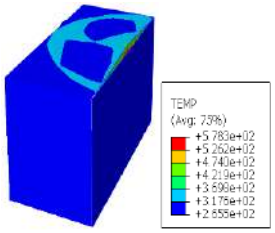
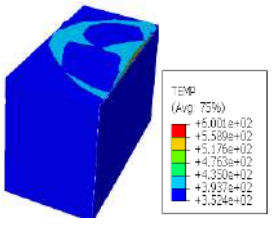
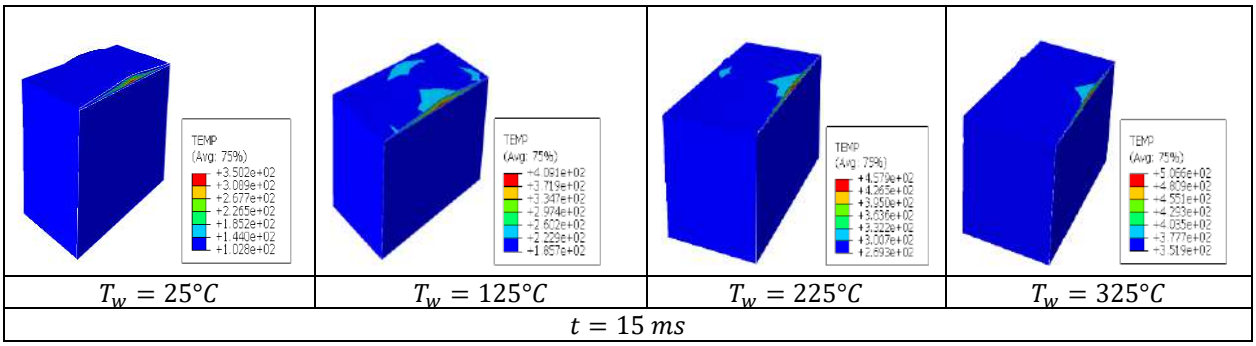


Figure IV.16. Transient Thermal Influence on the Solidification Thickness of Aluminum Droplets Impacting a Copper Substrate at 150 m·s⁻¹.

			
$T_w = 25°C$	$T_w = 125°C$	$T_w = 225°C$	$T_w = 325°C$
$t = 0.75mss$			
			
$T_w = 25°C$	$T_w = 125°C$	$T_w = 225°C$	$T_w = 325°C$
$t = 3.75\ ms$			
			
$T_w = 25°C$	$T_w = 125°C$	$T_w = 225°C$	$T_w = 325°C$
$t = 7.5\ ms$			



$T_w = 25°C$	$T_w = 125°C$	$T_w = 225°C$	$T_w = 325°C$
$t = 15\ ms$			

Figure IV.17. Temperature contour distribution for varying substrate temperatures.

The spreading behavior of droplets is highly sensitive to their impact velocity, as illustrated in Figure IV.17. As the velocity increases, the droplet experiences greater inertial forces, resulting in more pronounced deformation upon contact with the substrate. This enhanced deformation increases the contact area between the droplet and the substrate, which in turn promotes a higher rate of heat transfer from the droplet to the underlying material. Consequently, the thermal energy dissipates more rapidly, affecting both the cooling rate and the dynamics of solidification.

This relationship between impact velocity and thermal behavior is further substantiated by observations of the thickness of the resulting solidified layer. Figures IV.18 and IV.19 demonstrate a clear correlation: droplets impacting at higher velocities tend to form thinner solidified layers due to the more extensive spreading and accelerated heat dissipation, whereas lower-velocity droplets produce thicker layers because of limited deformation and slower thermal transfer. These findings highlight the coupled nature of mechanical and thermal phenomena during droplet impact, showing that droplet velocity not only influences macroscopic spreading but also governs microstructural characteristics, such as splat morphology and solidification patterns.

Understanding the effect of impact velocity is particularly critical for optimizing thermal spray processes, as it provides insights into controlling coating uniformity, adhesion strength, and microstructural properties. By quantifying the influence of velocity on spreading and solidification, this study contributes to the development of predictive models that can guide process parameters, ensuring consistent and high-quality coating deposition in industrial applications

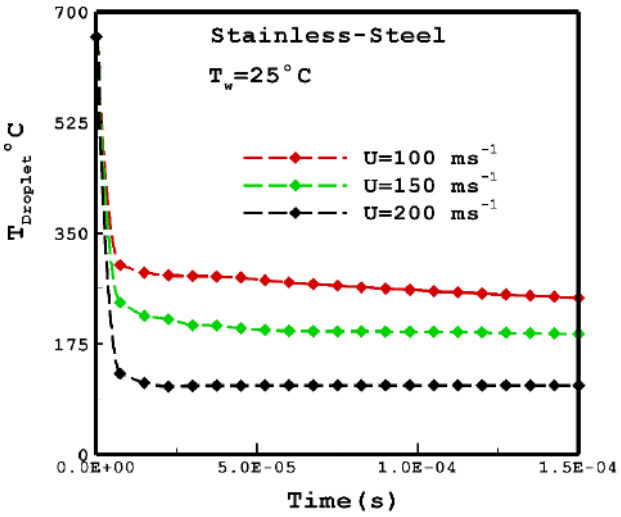


Figure IV.18. Temperature change over time of an aluminum droplet on a stainless steel substrate at different impact velocities, T_w=25°C.

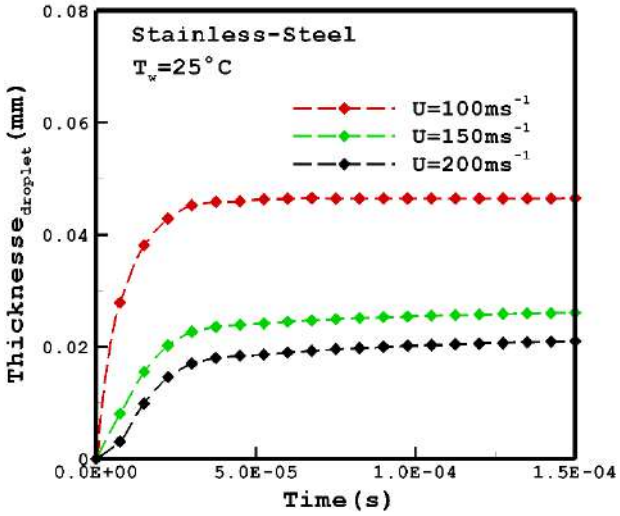


Figure IV.19. Changes in the thickness of the solidified layer over time of an aluminum droplet striking a stainless steel substrate at various speeds (T_w=25°C)

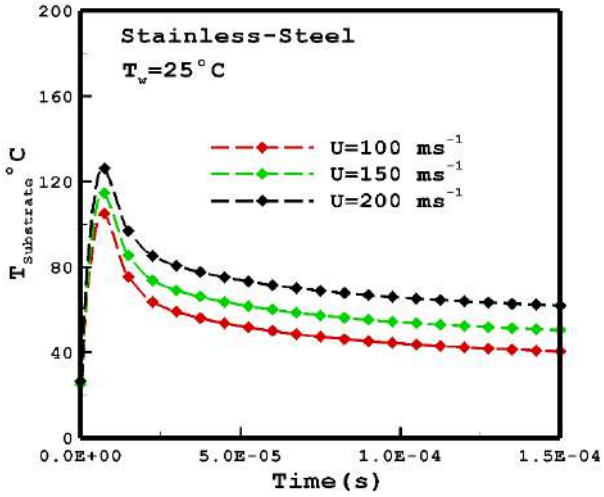


Figure IV.20. Stainless-steel substrate's temperature changes over time when aluminum droplets strike it at different speeds (T_w=25°C).

The relationship between substrate thermal conductivity and energy dissipation is further illustrated in Figure The spreading behavior of droplets is highly sensitive to their impact velocity, as illustrated in Figure IV.19 As the velocity increases, the droplet experiences greater inertial forces, resulting in more pronounced deformation upon contact with the substrate. This enhanced deformation increases the contact area between the droplet and the substrate, which in turn promotes a higher rate of heat transfer from the droplet to the underlying material. Consequently, the thermal energy dissipates more rapidly, affecting both the cooling rate and the dynamics of solidification, which demonstrates that materials with superior conductivity dissipate thermal energy more efficiently, leading to faster stabilization of droplet temperature. In contrast, substrates with lower thermal conductivity retain heat for longer periods, resulting in a slower cooling rate and more gradual solidification. This behavior underscores the importance of selecting appropriate substrate materials when precise control over droplet solidification and coating properties is required.

Figure IV.23 complements these observations by presenting the temporal evolution of temperature contours across the different substrate grades. These contours provide a visual representation of how heat spreads within the substrate and how it influences the thermal gradients in the droplet during impact and spreading. Substrates with higher conductivity exhibit steeper thermal gradients and faster energy dissipation, while lower-conductivity materials show more diffuse temperature distributions.

Overall, these findings emphasize that substrate selection is not merely a boundary condition but a decisive factor in controlling heat transfer, solidification dynamics, and ultimately the quality and structural characteristics of thermally sprayed coatings. Understanding the interplay between droplet properties and substrate thermal behavior is essential for optimizing process parameters and achieving desired coating performance in industrial applications.

The dissipation of thermal energy from a molten droplet is fundamentally governed by the substrate's material properties, particularly its specific heat capacity and thermal conductivity. Figure IV.21 highlights the critical influence of substrate grade on heat transfer during droplet impact. Materials with higher thermal conductivity, such as copper, facilitate more rapid heat extraction from the droplet compared to substrates like stainless steel or nickel. This enhanced thermal transport accelerates droplet cooling and influences the kinetics of solidification, ultimately affecting the morphology and microstructure of the splat.

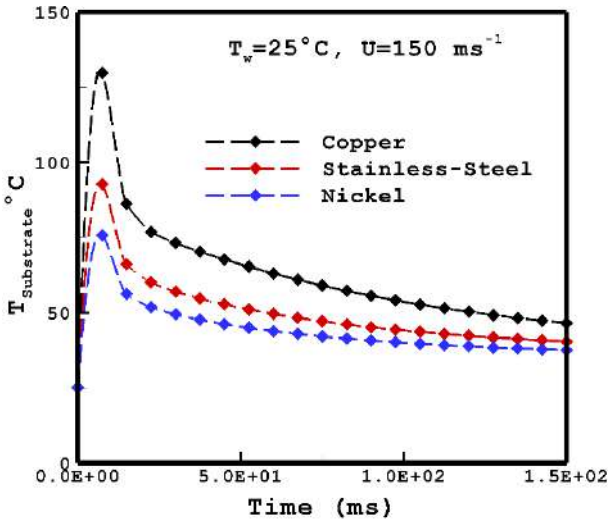


Figure IV.21. Temporal evolution of the temperature of substrates of different grades subjected to aluminum droplet impact.

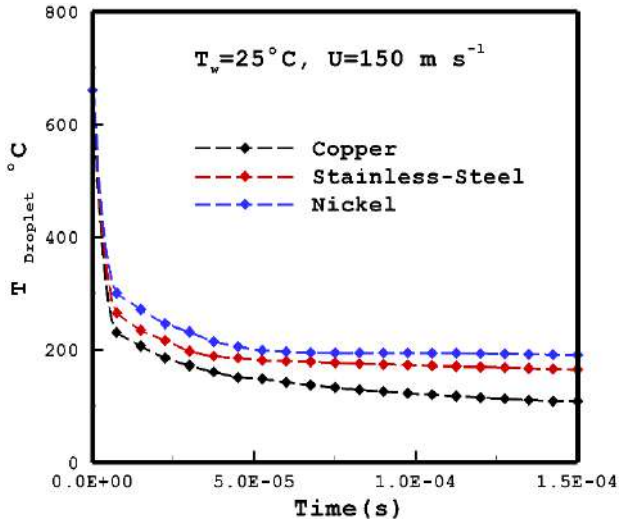
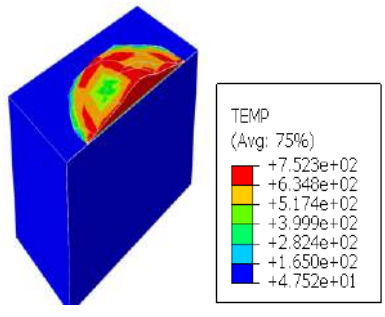
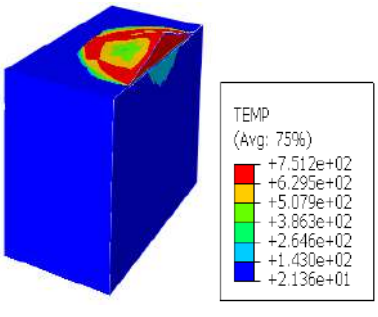
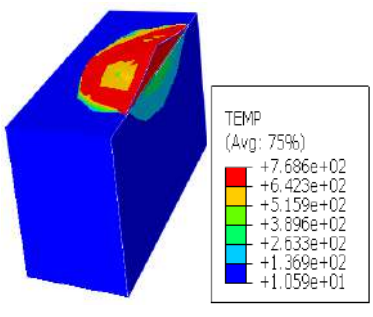


Figure IV.22. Temporal evolution of the temperature of an aluminum droplet impacting various substrate materials ($U = 150\, ms^{-1}, T_w = 25\, °C$).

		
Stainless-steel	Cooper	Nickel
$t = 0.75\, ms$		

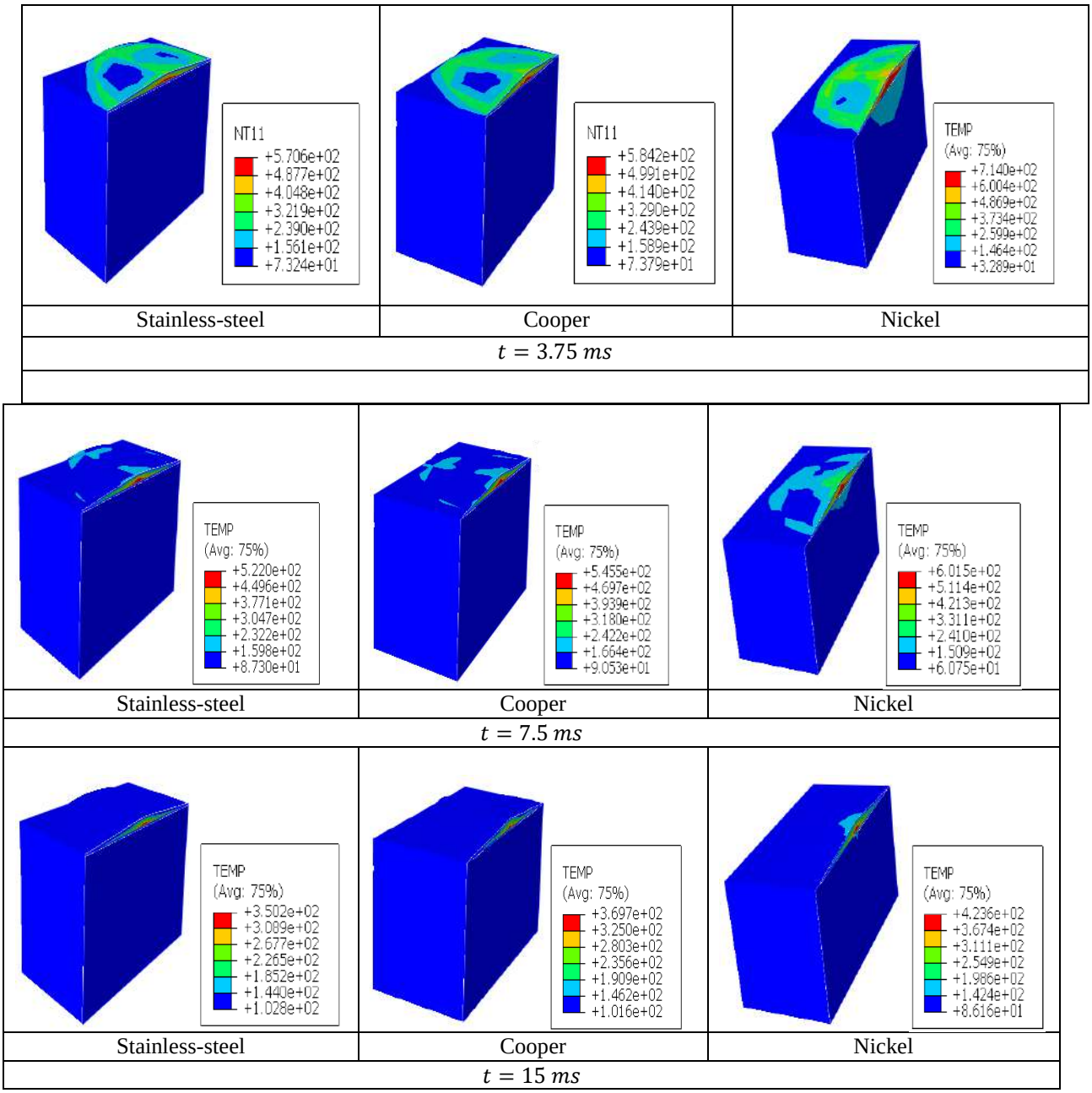


Figure IV.23. Temperature contour distribution for various substrate grades.

Figure IV.24 illustrates that the thickness of the solidified zone within the droplet exhibits minimal variation over time, regardless of the initial substrate temperature. This limited influence can be attributed to the fact that, in all cases, the substrate temperature remains below the melting point of the droplet's base metal, thereby restricting any significant heat feedback from the substrate to the droplet. Consequently, the rate and extent of solidification are primarily governed by the droplet's intrinsic thermal properties and the energy dissipated during spreading, rather than by minor variations in the substrate's initial thermal state.

In contrast, the metallurgical composition and grade of the substrate have a substantially stronger effect on the solidified layer's thickness, as evidenced in Figure IV.25. Substrates with

higher thermal conductivity, such as copper, promote more rapid heat extraction from the droplet, leading to thinner solidified zones, whereas materials with lower conductivity, like stainless steel or nickel, result in comparatively thicker solidified layers. This observation underscores the critical role of substrate material selection in influencing solidification kinetics and controlling the microstructural characteristics of the deposited splat.

These findings highlight that, while initial substrate temperature exerts a relatively minor influence under the tested conditions, the intrinsic thermal and metallurgical properties of the substrate are decisive factors in determining the evolution of the droplet's solidified layer. Such insights are particularly valuable for thermal spray applications, where careful consideration of substrate material can directly impact coating quality, adhesion, and structural integrity.

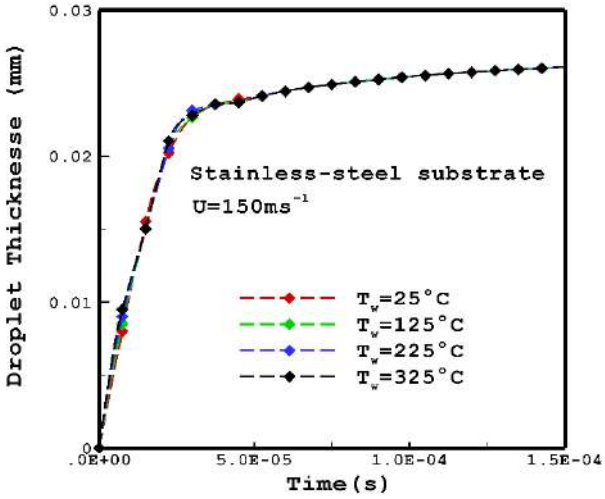


Figure IV.24. Evolution of the solidification thickness of an Aluminum droplet on a stainless-steel substrate at variable temperatures

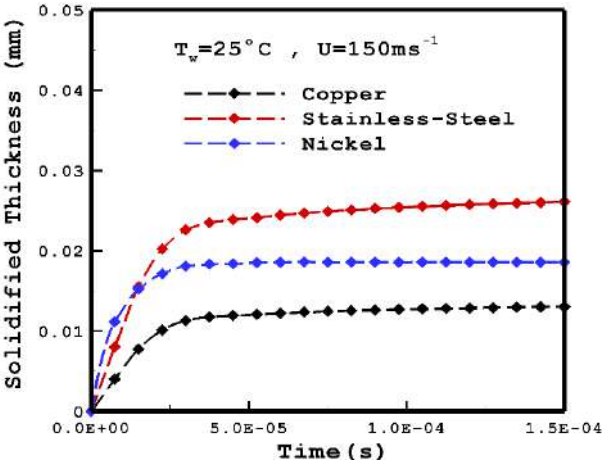


Figure IV.25. Evolution of the solidification thickness of an Aluminum droplet on Substrates of varying grades.

VI.3. SECOND SECTION, A MULTIPARTICLE SYSTEM.

To gain a more comprehensive understanding of droplet interactions and solidification dynamics during thermal spraying, a study was conducted examining the successive impact of three superimposed particles. This approach allows for the investigation of cumulative effects on particle flattening, heat transfer, and solidification, which cannot be fully captured by single-particle analyses. By analyzing the sequential deposition of multiple droplets, the study provides insights into the interaction between previously deposited layers and incoming particles, including potential remelting, overlapping splat formation, and variations in local cooling rates.

Figures IV.26 and IV.27 illustrate the results of this investigation, highlighting both the morphological evolution of each droplet and the thermal gradients established across the stacked layers. The first particle behaves similarly to single-particle impacts, spreading upon contact and gradually solidifying. The second and third particles, however, encounter a substrate that is partially preheated and modified by the previous impacts. This preheating influences the rate of heat extraction, causing subtle variations in the extent of spreading and solidification compared to the initial droplet. Furthermore, the overlapping particles interact thermally, leading to a more complex distribution of temperature and solidification fronts, which is critical for understanding layer adhesion, coating density, and microstructural uniformity.

By studying the sequential deposition of multiple particles, this analysis captures essential phenomena relevant to industrial thermal spray processes, where coatings are built up layer by layer. The findings emphasize the importance of considering cumulative thermal and mechanical effects in predictive models, as these factors significantly affect the final coating morphology, thickness, and microstructural properties. Such knowledge is essential for optimizing process parameters and achieving high-quality, uniform coatings in practical applications

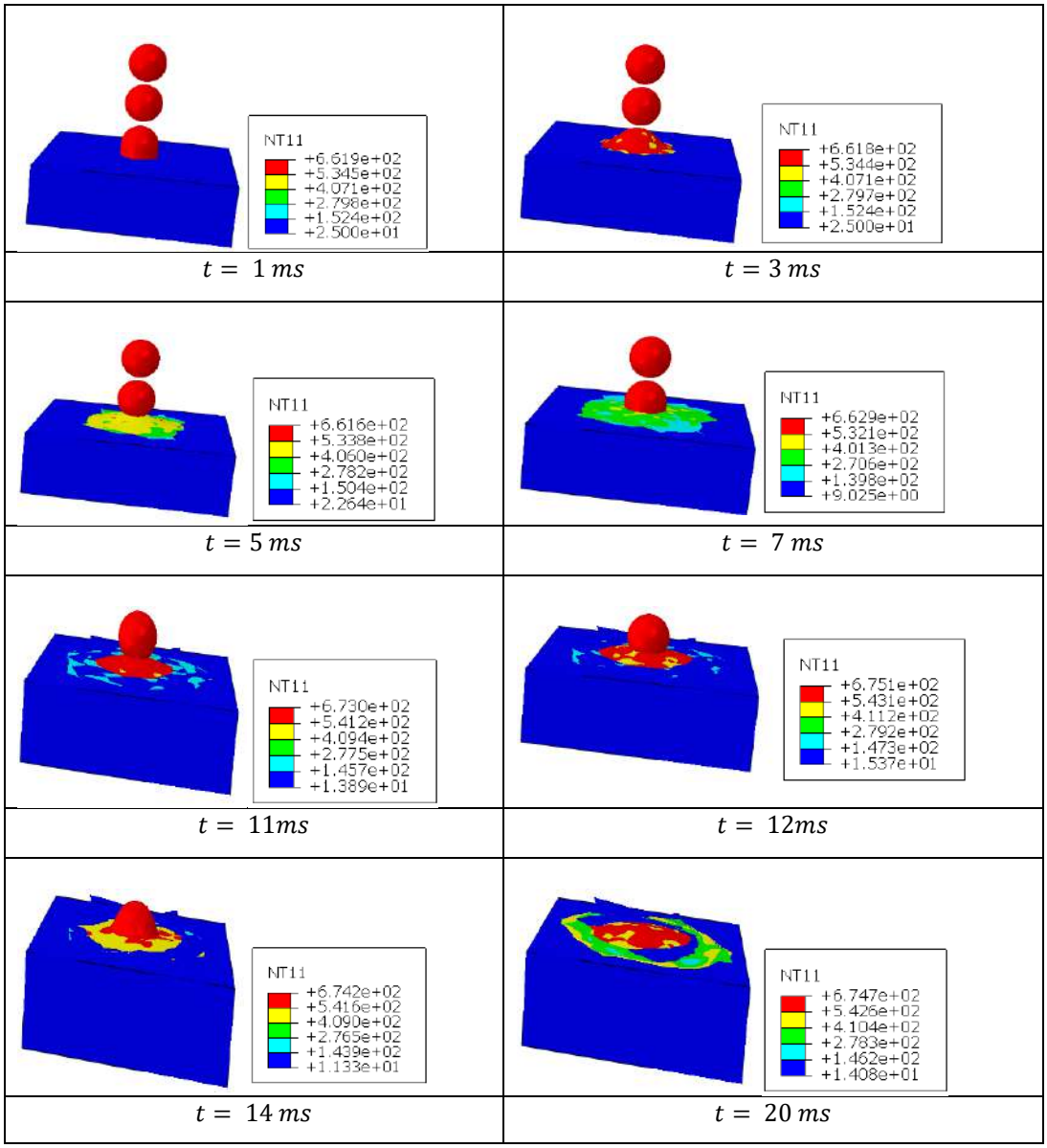


Figure IV.26. Temperature Contour Mapping for a Multi-Particle Impacts.

Figure IV.26 presents the temporal evolution of temperature contours during the successive impacts, providing a detailed visualization of heat distribution throughout the substrate and the deposited particles. Figure IV.27, in turn, illustrates the solidification process of the three sequentially deposited particles, highlighting the interactions between layers and the progression of phase transitions. The first particle impacts the bare substrate directly, spreading and solidifying according to the substrate's initial thermal conditions. The second particle then lands on the already flattened and partially solidified surface of the first particle, while the third particle follows the same deposition pattern, interacting with the thermally and mechanically altered surface beneath it.

Each successive impact modifies the local substrate temperature and thermal gradients, affecting the rate of heat dissipation for subsequent particles. As a result, the second and third particles experience a substrate that is preheated and partially deformed, leading to variations in spreading behavior, cooling rates, and solidification dynamics compared to the initial particle. The cumulative thermal and mechanical interactions between the layers are critical for understanding coating formation, as they influence not only the thickness and morphology of each splat but also interlayer adhesion, microstructural uniformity, and residual stress development.

These observations emphasize that in multilayer thermal spray processes, each new particle interacts with a dynamically evolving surface, and the resulting thermal history is a complex superposition of previous impacts. Understanding these sequential interactions is essential for accurate modeling, optimization of process parameters, and the production of high-quality, uniform coatings with desirable mechanical and microstructural properties.

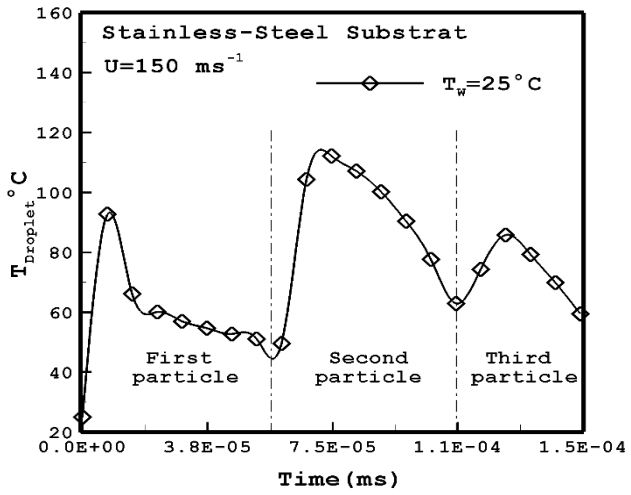


Figure IV.27: Temporal variation of substrate temperature during the impact of three particles.

IV.4. THIRD SECTION: ELLIPTICAL SHAPE OF THE DROPLET

The curve (figure VI.28) highlights a rapid thermal rise followed by a gradual decay toward a quasi-steady regime.

Before impact, the aluminum particle significantly superheated relative to its melting temperature comes into contact with a substrate initially at 25 °C, thereby generating a strong thermal gradient. Upon contact, the droplet spreads rapidly under the effect of its inertia, forming an elliptical splat. The interaction between the liquid metal and the solid surface induces an intense conductive heat transfer, initially concentrated over a very small area. This

configuration results in a sharp increase in the substrate's surface temperature, which reaches approximately 80 °C within a few microseconds, while the particle remains largely in the liquid state.

The observed temperature peak arises from the combined effects of an already well-developed contact area, a still dominant heat flux from the particle to the substrate, and the onset of heat diffusion into the stainless-steel bulk, which further limits the surface temperature rise. Subsequently, the temperature decrease is governed by the progressive solidification of the aluminum (accompanied by the release of latent heat) as well as by the three-dimensional diffusion of thermal energy into the substrate, ultimately leading to stabilization around 50 °C. By the end of the process, the solidified particle reaches a temperature close to that of the substrate, and thermal dissipation is controlled by conduction within the steel and by convective and radiative exchanges with the surroundings.

The elliptical geometry of the particle plays a decisive role in this thermal behavior. It produces a larger contact area than a spherical droplet of equivalent volume, thereby enhancing heat transfer efficiency and accelerating solidification. This geometry also distributes the thermal field over a wider lateral region and modifies the subsurface temperature gradients, which become less pronounced than in the case of a nearly point-like impact.

Within the framework of thermal spray processes, these observations fit into an energy balance in which the particle transfers a significant fraction of its sensible and latent heat to the substrate. The substrate's thermal response can be approximated by a semi-infinite solid model, whose transient conduction behavior typically exhibits a surface temperature peak followed by a decay proportional to the inverse of time. This thermal regime has direct implications for coating adhesion and quality: a rapid yet controlled increase in substrate temperature enhances the wettability of liquid aluminum and promotes the formation of a dense, well-anchored splat. Finally, the strong thermal gradient induces rapid cooling, favoring the development of a fine microstructure within the deposit and potentially improving its mechanical performance.

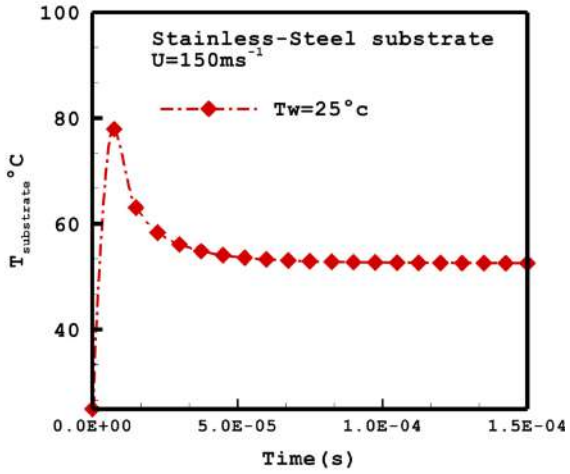


Figure IV.28. Evolution of the Temperature of a Stainless-Steel Substrate (T_0 = 25 °C) During the Impact of an Elliptical Aluminum Particle at 150 m/s

The graph (figure IV.29) illustrates the rapid decrease in temperature of an aluminum particle initially superheated between 660°C, close to its melting point, down to approximately 100 °C at the end of the process, beginning with an extremely fast drop upon initial contact with the stainless-steel substrate at 25 °C, which generates an intense, conduction-driven heat transfer concentrated over the contact area and induces a severe cooling of the particle at rates on the order of 10^6 to 10^7 K/s, typical of thermal spray processes, followed by a solidification phase initiated around 300–400 °C due to undercooling, during which the release of latent heat slightly moderates the temperature decay, and then a final cooling phase in which the temperature decreases more slowly and asymptotically approaches an equilibrium value of approximately 100 °C, controlled by three-dimensional heat diffusion within the substrate and the thermal contact resistance at the particle/substrate interface, while the elliptical geometry of the particle significantly increases the contact area compared to a sphere of equivalent volume, enhancing heat transfer efficiency, accelerating solidification, and promoting the formation of flatter, better-adhered splats, which in turn results in a fine-grained microstructure, induces residual stresses due to differential thermal contraction between aluminum and stainless steel, and strongly influences the final coating adhesion through the interface thermal resistance, thereby reflecting the full range of thermal and metallurgical phenomena that determine the quality and performance of a deposit produced by thermal spraying.

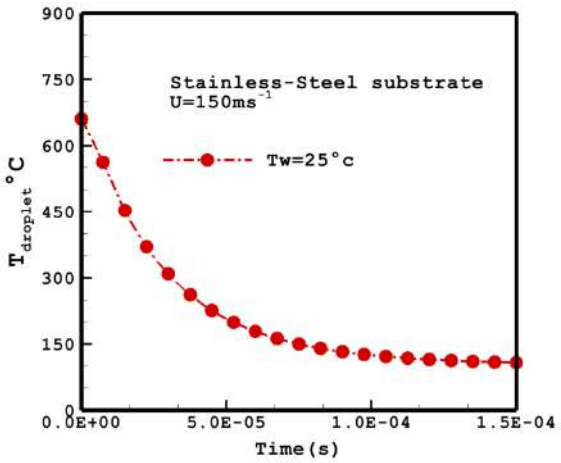


Figure IV.29. Temperature Evolution of an Elliptical Aluminum Particle Impacting a Stainless-Steel Substrate (T_0 = 25 °C) at 150 m/s.

The graph IV.30. illustrates the temporal evolution of the thickness of a solidified elliptical pure aluminum droplet on a stainless-steel substrate at 25 °C during an impact at 150 m/s. The vertical axis represents the thickness of the solidified deposit (in meters), while the horizontal axis corresponds to the elapsed time after impact (in seconds). Initially, the thickness increases rapidly up to approximately 0.015 m, followed by a plateau where it remains nearly constant.

From a physical perspective, this behavior can be explained by the fact that, at the very beginning of contact, only a thin layer of aluminum in direct contact with the substrate solidifies, resulting in an initially negligible solid thickness. As heat is extracted toward the much colder substrate by conduction, the solidification front progresses rapidly within the droplet, causing the steep increase in thickness during the first microseconds. Once the entire elliptical droplet has solidified, the thickness reaches its maximum and stabilizes, with subsequent cooling of the solid splat and heat diffusion into the substrate affecting only the internal temperature without altering the thickness.

The elliptical shape of the particle plays a critical role in this process: compared to a sphere of equivalent volume, it spreads more extensively, producing a wider and thinner deposit with a high surface-to-volume ratio, which promotes rapid heat extraction and accelerated solidification. This configuration leads to a fine-grained microstructure within the splat, directly influencing the hardness, residual stresses, and adhesion of the coating to the stainless-steel substrate.

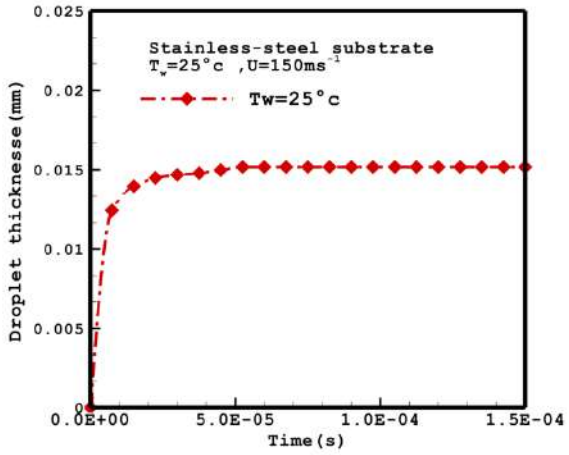


Figure IV.30. Temporal Evolution of the Thickness of a Solidified Elliptical Aluminum Droplet on a Stainless-Steel Substrate (T_0 = 25 °C) During Impact at 150 m/s.

The graph (figure IV.31) presents a comparison of the surface temperature evolution of a stainless-steel substrate during the impact of two pure aluminum particles projected at 150 m/s, one elliptical and the other spherical. The vertical axis represents the substrate temperature $T_{substrate}$ in °C, while the horizontal axis indicates the elapsed time after impact in milliseconds. The black dashed curve corresponds to the elliptical particle, and the red dashed curve to the spherical particle. In both cases, the substrate temperature rises rapidly to a peak and then gradually decreases, stabilizing at a few tens of degrees above the initial temperature.

From a physical perspective, at the moment of contact, the liquid aluminum is significantly superheated above 660 °C, whereas the substrate is initially near 25 °C, generating a strong thermal gradient and an intense heat flux from the droplet to the substrate, which explains the rapid increase in $T_{substrate}$during the first tens of microseconds. The temperature peak corresponds to the instant when the heat flux is maximal, prior to the distribution of energy throughout the substrate volume. Subsequently, heat propagates into the substrate (transient conduction in a semi-infinite solid), causing a progressive decrease in surface temperature toward a plateau slightly above the initial temperature. During this phase, the aluminum droplet solidifies and releases its latent heat of fusion, while the heat flux progressively decreases as the thermal gradient diminishes.

The particle shape significantly influences this thermal behavior. For the elliptical particle, the contact area with the substrate is larger, spreading the heat flux over a wider region and producing a very high initial temperature rise of short duration, followed by a rapid cooling of the impacted zone. In contrast, for the spherical particle, the smaller contact area concentrates

heat on a more restricted region, yielding a slightly different temperature peak and a slower decay, as heat diffuses more gradually.

Within the context of thermal spray processes, these observations highlight the sensitivity of the substrate thermal field to particle geometry: a flattened (elliptical) shape promotes rapid heat extraction, accelerated solidification of the splat, and a finer microstructure, whereas a compact (spherical) geometry induces localized thermal gradients that may generate different residual stresses in the final coating.

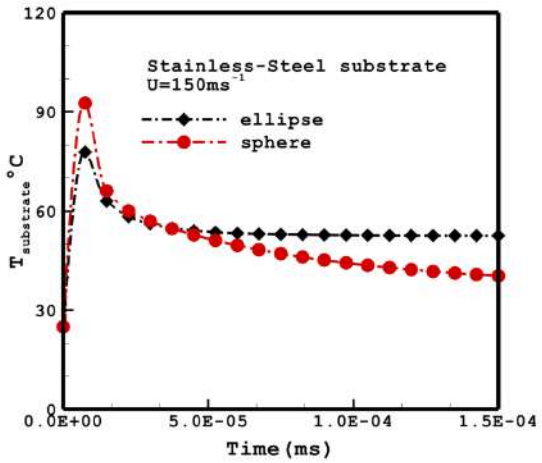


Figure IV.31. Comparison of Temperature Evolution of a Stainless-Steel Substrate During the Impact of Two Aluminum Particles at 150 m/s.

The graph (Figure IV.32) illustrates the temperature decay of two pure aluminum droplets (one elliptical and the other spherical) during their impact on a stainless-steel substrate at 150 m/s, as a function of time after contact. The vertical axis represents the droplet temperature T_{drolet} in °C, while the horizontal axis indicates time in milliseconds. The red diamond-marked curve corresponds to the elliptical particle, initially at approximately 670 °C and cooling down to around 100 °C, whereas the black circle-marked curve represents the spherical particle, which starts at a lower temperature (~250 °C) and stabilizes around 200 °C.

From a physical standpoint, upon impact, the liquid aluminum rapidly transfers heat to the cold substrate via conduction, inducing a sharp cooling of the droplet with rates typically on the order of 10^6–10^7 K/s in thermal spray processes. The droplet spreads to form a splat, while solidification progresses from the substrate droplet interface inward. The release of latent heat of fusion temporarily moderates the slope of the temperature decay. Once the droplet is fully solidified, the temperature continues to decrease more slowly, governed by heat diffusion into the substrate and exchange with the surrounding environment.

Particle geometry strongly influences this thermal behavior. For the elliptical droplet, the larger contact area and higher surface-to-volume ratio enhance heat extraction, explaining the rapid cooling and the drop to ~100 °C. In contrast, the spherical droplet, with a smaller contact area, concentrates the heat flux over a restricted region, resulting in a slower temperature decline and a higher final temperature (~200 °C), indicating reduced energy loss to the substrate.

Within the context of thermal spray processes, these results highlight the impact of particle geometry on thermal history: the elliptical particle solidifies faster and reaches a lower final temperature, promoting a very fine microstructure but also significant residual stresses in the aluminum splat on the substrate, whereas the spherical particle, remaining hotter, may solidify more slowly, produce a slightly coarser microstructure, and exhibit a different thermal coupling with the substrate, thereby affecting coating adhesion and final properties.

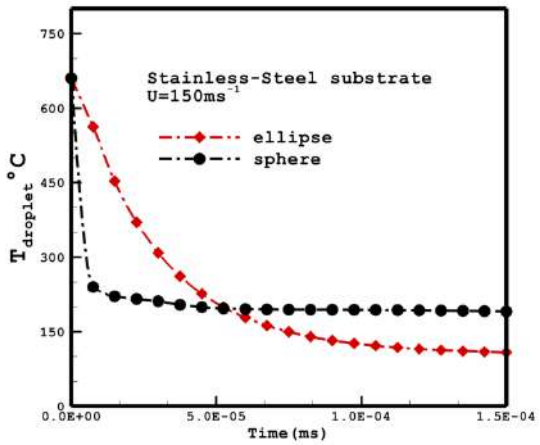


Figure IV.32. Temperature Decay of Elliptical and Spherical Aluminum Droplets During Impact on a Stainless-Steel Substrate at 150 m/s

The graph (Figure IV.33) presents a comparison of the evolution of the solidified thickness of two pure aluminum droplets (one elliptical and the other spherical) projected at 150 m/s onto a stainless-steel substrate initially at 25 °C. The vertical axis represents the droplet thickness in millimeters, while the horizontal axis indicates the elapsed time after impact in seconds. The red triangle-marked curve corresponds to the elliptical droplet, stabilizing around 0.02 mm, whereas the black diamond-marked curve represents the spherical droplet, reaching a larger final thickness of approximately 0.035–0.04 mm. In both cases, the thickness increases rapidly immediately after impact and then levels off, forming a plateau corresponding to the final thickness of the solidified splat.

Physically, upon impact, the liquid droplet strikes the substrate at high velocity and spreads radially to form a splat. The portion in contact with the substrate cools rapidly by conduction and begins to solidify, causing a fast growth of the solidified thickness during the first tens of microseconds, as indicated by the steep rises of the curves. Once the droplet is nearly fully solidified, the progression of the solid–liquid front ceases, the thickness stabilizes, and subsequent cooling affects only the internal temperature and microstructure of the deposit.

Particle geometry strongly influences this behavior. The elliptical droplet spreads more at equivalent volume, producing a wider but thinner deposit, with a plateau at ~0.02 mm; its higher surface-to-volume ratio promotes rapid heat extraction and uniform solidification. In contrast, the spherical droplet retains a more compact shape, spreads less, and forms a thicker deposit (~0.035–0.04 mm), with heat being extracted over a smaller area, slightly slowing solidification and increasing the thermal gradient through the thickness.

In the context of thermal spray processes, these results demonstrate that particle shape directly controls the final splat thickness and, consequently, the local microstructure of the coating: elliptical droplets tend to produce thin, fine-grained layers with rapid solidification, whereas spherical droplets lead to thicker deposits, more pronounced thermal gradients, and potentially different residual stresses within the aluminum coating on the stainless-steel substrate.

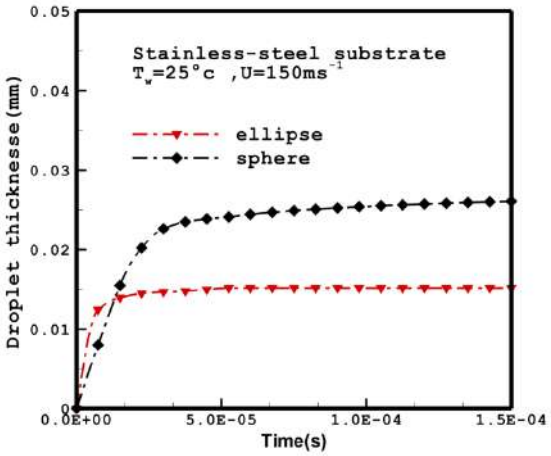


Figure IV.33. Comparison of Solidified Thickness Evolution of Elliptical and Spherical Aluminum Droplets Impacting a Stainless-Steel Substrate at 150 m/s.

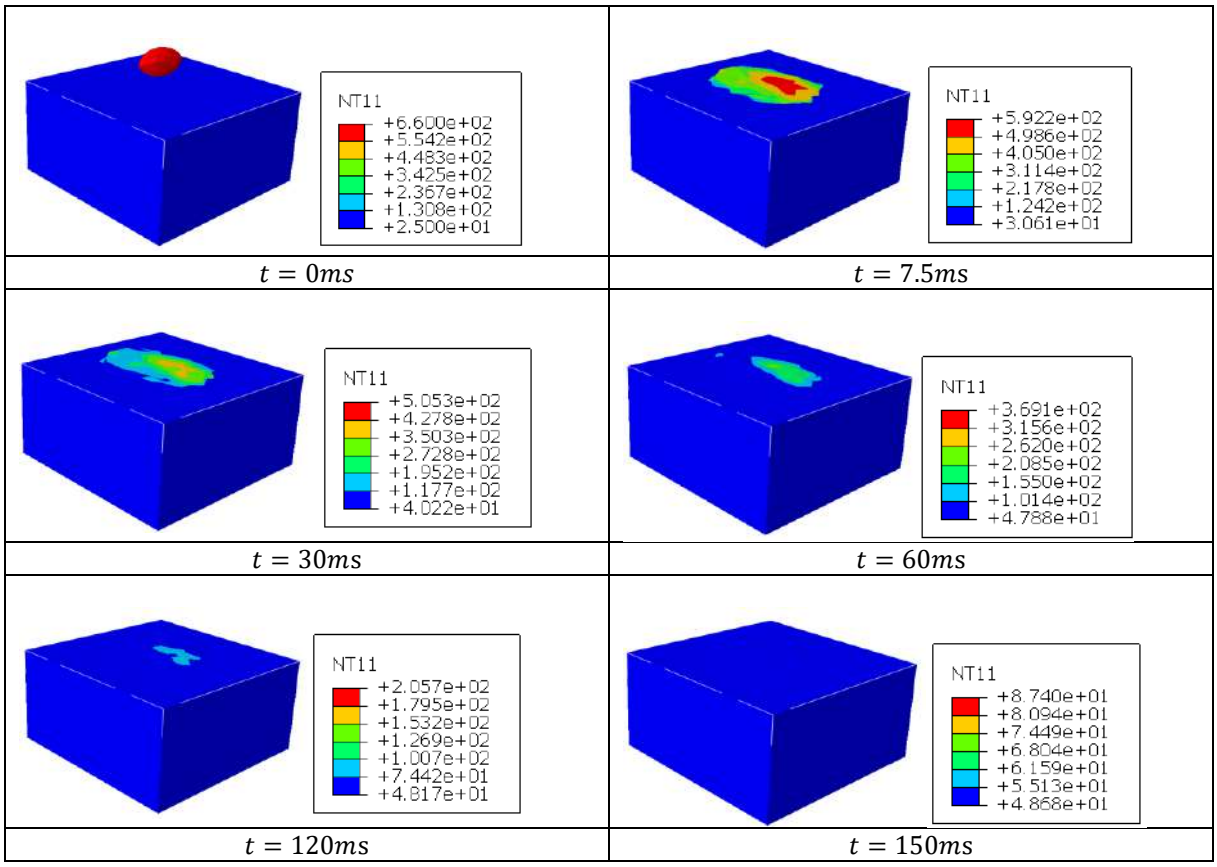


Figure IV.34. Temperature Contours Generated by the Impact of an Elliptical Particle.

The figure VI.34 shows how the temperature field and the shape of the elliptical droplet evolve over time, offering a kind of real time view of what happens during impact. It makes it possible to clearly see how heat spreads at the droplet substrate interface, as well as how the droplet deforms under the combined effects of impact and rapid solidification. Through this time-resolved visualization, the complex interplay between thermal conduction, heat transfer, and fluid flow becomes more tangible, shedding light on the solidification kinetics and the way the final splat is formed. By comparing these results with those obtained for droplets of different shapes, one can better assess how geometry affects thermal diffusion and deposit stability, which is crucial for optimizing thermal spray operating conditions and predicting the resulting coating properties.

IV.5. CONCLUSION:

Overall, the numerical analyses conducted on the impact of superheated pure aluminum droplets on a stainless-steel substrate at 150 m/s provide a detailed picture of the coupled thermal and solidification phenomena governing splat formation in thermal spray processes. The results show that, for an elliptical particle, the substrate surface temperature exhibits a rapid

rise followed by a decay toward a quasi-steady regime, while the droplet itself cools at rates on the order of 10^6–10^7 K/s and undergoes fast solidification, leading to a stable splat thickness. The comparison between elliptical and spherical particles highlights the decisive influence of geometry: the elliptical droplet, with its larger contact area and higher surface-to-volume ratio, enhances conductive heat transfer, accelerates solidification, reduces temperature gradients within the deposit, and promotes the formation of thin, flat splats with a fine microstructure. In contrast, the spherical particle generates thicker deposits, more localized thermal gradients, and a different residual stress state.

From an applied standpoint, these findings underscore the critical role of particle morphology in controlling the thermal history of both droplet and substrate, the kinetics of solidification, and the final splat geometry. They demonstrate that accounting for non-spherical droplet shapes can significantly improve the fidelity of numerical models and contribute to a more rational optimization of thermal spray parameters. Ultimately, this work shows that the shape of impacting particles is not a secondary detail, but a key design parameter for tailoring coating adhesion, microstructure, and mechanical performance in advanced thermal spray applications.

IV.6. GENERAL CONCLUSION

In this work, the deformation and spreading of a single aluminum droplet were simulated to establish a representative model of the thermal spraying process. Unlike approaches that treat the particle as a weakly bonded solid, a fully coupled thermo-mechanical framework was employed, in which the droplet was modeled as a fluid with temperature-dependent properties. The governing equations were solved using ABAQUS/Explicit, allowing for high-resolution, time-accurate simulations of impact dynamics, heat transfer, and phase transition phenomena. This approach enabled a detailed examination of the complex interactions between the droplet and the substrate during impact, spreading, and solidification.

The key findings of this simulation can be summarized as follows:

- **Viscous characteristics of molten aluminum**: The rheological properties of the droplet proved suitable for accurately modeling spreading, deformation, and energy dissipation during impact. The fluid-based approach captured the dynamic flow behavior and flattening processes that occur immediately upon contact.

- **Temperature-dependent material properties**: Incorporating temperature-dependent variations in density, specific heat, thermal conductivity, and viscosity provides a more realistic representation of droplet behavior, particularly in relation to thermal gradients and solidification kinetics.
- **Variable thermal contact conductance**: The introduction of a variable thermal contact conductance significantly affects the formation of lamellae (splats) and the efficiency of heat transfer between the droplet and substrate. This parameter governs the local cooling rate and influences adhesion mechanisms.
- **Impact dynamics and velocity effects**: The particle's velocity at the moment of impact strongly determines spreading, splat morphology, and the effectiveness of adhesion. Higher velocities lead to greater deformation, larger contact areas, and enhanced heat transfer, whereas lower velocities result in thicker splats and slower solidification.
- **Tribological interactions**: Frictional effects at the droplet–substrate interface contribute to energy dissipation and assist in anchoring the particle, influencing both mechanical interlocking and thermal energy distribution.
- **Surface roughness and material compatibility**: The roughness of the substrate, as well as the metallurgical compatibility between particle and substrate alloys, plays a decisive role in the final coating quality. These factors influence adhesion, splat morphology, and the uniformity of deposited layers.
- **Validation with experiments and prior simulations**: The outcomes of the present model align closely with experimental observations and previous numerical studies, demonstrating its reliability for predicting droplet behavior under varying thermal and mechanical conditions.

Taken together, these results indicate that the proposed model provides a comprehensive and physically realistic framework for analyzing single-particle impact during thermal spraying. It can serve as a robust foundation for future studies exploring the influence of substrate surface conditions, droplet size, and the number of particles on lamella formation, coating microstructure, and overall deposition quality. By incorporating coupled thermal, mechanical, and tribological phenomena, the model facilitates predictive insights into coating design, process optimization, and material performance in industrial applications.

IV.7. PERSPECTIVES

Building upon the findings of this study, several avenues for future research can be identified to further enhance the understanding and predictive capability of droplet impact phenomena in thermal spraying:

- Integration of oxidation and chemical reactions including models for oxidation, intermetallic formation, or surface chemistry at the droplet–substrate interface would offer deeper insight into adhesion mechanisms, especially for metallic systems that undergo rapid high-temperature reactions during impact.
- Advanced modeling of substrate conditions Incorporating realistic surface topographies including roughness profiles, grooves, and asperity distributions would allow for better assessment of mechanical interlocking. Similarly, simulating substrates with temperature gradients or heterogeneous material properties could capture more accurately the behavior encountered in industrial applications.
- Coupled fluid-solid multiphysics simulation extending the model to account for elastic–plastic deformation of the substrate, substrate melting, and solid–liquid interactions may improve predictions of interfacial bonding and splat morphology, especially for high-velocity and high-temperature process variants.
- Consideration of vaporization and phase explosion phenomena at extreme particle temperatures or in plasma spraying conditions, mechanisms such as vapor entrapment, splashing, and micro-explosions become relevant. Incorporating these effects would broaden the model's applicability to a wider range of thermal spray processes.
- Parameter optimization using machine learning the combination of high-fidelity simulations and data-driven approaches could help optimize process parameters (particle temperature, velocity, stand-off distance, substrate preparation) to achieve targeted coating properties with improved efficiency.
- Experimental coupling and validation additional high-speed imaging, infrared thermography, and post-impact characterization (SEM, profilometry, metallography) would strengthen model validation and support the refinement of material parameters used in simulations.
- Scale-up toward industrial process simulation integrating the single-droplet model within a larger computational framework including full spray plume dynamics, torch–substrate interactions, and thermal-cycle histories would provide a path toward digital twins for real-time monitoring and predictive control of thermal spray manufacturing.

- Extend this study by examining the impact of droplets with various shapes (elliptical, spherical, and combined) on different types of substrates, including composite or functionalized materials. Such an investigation would provide a deeper understanding of the combined influence of particle morphology and substrate properties on thermal distribution, solidification kinetics, and the formation of multilayer deposits. Moreover, this work could pave the way for the development of more accurate predictive models, capable of guiding the optimization of thermal spray parameters to achieve more uniform, durable coatings tailored to specific industrial applications.

Bibliography :

[1] A. Benmokhtar, «Préparation de surface pour la projection thermique», thèse de doctorat, Université de technologie de Belfort-Montbéliard, 2011.thesis.univ-biskra

[2] F. Chouit, «Étude bibliographique et expérimentale des procédés de projection thermique (projection plasma de revêtements Ni–Al et Al_2O_3)», mémoire de Magister, Université Badji Mokhtar Annaba.biblio.univ-annaba

[3] G. Marot, «Détermination de l'adhérence de revêtements obtenus par projection thermique», thèse de doctorat, Université de Lille 1, 2007.pepite-depot.univ-lille

[4] Thèse Univ. Limoges, «Élaboration par projection thermique d'éléments finement structurés…», Université de Limoges, 2010 (torche plasma, phénomènes physiques de projection).unilim

[5] Y. Fizi, «Analyse par simulation numérique du comportement de dépôts obtenus par projection thermique», thèse de doctorat, Université de Sétif.dspace.univ-setif

[6] W. Liu, G.X. Wang, and E.F. Matthys,"Thermal Analysis and Measurements for a Molten Metal Drop Impacting on a Substrate: Cooling, Solidification and Heat Transfer Coefficient,"International Journal of Heat and Mass Transfer., vol. 38, no. 8, pp. 1387-1395, May. 1995.

[7] K.K. Subedi, and S.C Kong,"Particle-Based Approach for Modeling Phase Change and Drop/wall Impact at Thermal Spray Conditions," International Journal of Multiphase Flow., vol. 165, p. 104472, August. 2023.

[8] M. Passandideh-Fard, R. Bhola, S. Chandra, and J. Mostaghimi,"Deposition of Tin Droplets on a Steel Plate: Simulations and Experiments,"International Journal of Heat and Mass Transfer., vol. 41, no.19, pp. 2929-2945, October. 1998.

[9] S. Attari, R. Rebhi, A. Abdellah El-Hadj, O.M. Ikumapayi, A.Q. Al-Dujaili, A.I. Abdulkareem, A.J. Humaidi, G. Lorenzini, and Y. Menni,"Thermo-Mechanical Modeling and Simulation of Impact and Solidification of an Aluminum Particle,"Mathematical Modelling of Engineering Problems.,vol.10, no. 2, pp. 389-397, April. 2023.

[10] S.D. Aziz, and S. Chandra,"Impact, recoil and splashing of molten metal droplets,"International Journal of Heat and Mass Transfer., vol. 43, no. 16, pp. 2841–

2857, August. 2000.

[11] G. Trapaga, E.F. Matthys, J.J. Valencia, and J. Szekely,“Fluid Flow, Heat Transfer, and Solidification of Molten Metal Droplets Impinging on Substrates: Comparison of Numerical and Experimental Results,”Metallurgical Transactions B.,vol. 23, no. 6,pp. 701-718, December. 1992.

[12] D. Attinger, Z. Zhao, and D. Poulikakos,“An Experimental Study of Molten Microdroplet Surface Deposition and Solidification: Transient Behavior and Wetting Angle Dynamics,”Journal of Heat Transfer.,vol. 122, no. 3, pp. 544-556, April. 2000.

[13] M.V. Gielen, R. de-Ruiter, R.B.J. Koldeweij, D. Lohse, J.H. Snoeijer, and H. Gelderblom,“Solidification of liquid metal drops during impact,”J. Fluid Mech., vol. 883, no. (A32),pp. 1-20, January. 2020.

[14] Y. Zhang, S. Matthews, and M. Hyland,“Role of Solidification in the Formation of Plasma Sprayed Nickel Splats Through Simulation and Experimental Observation,”International Journal of Heat and Mass Transfer.,vol.115, pp. 488-501, December. 2017.

[15] E. Dalir, A. Dolatabadi, and J. Mostaghimi,“Modeling the Effect of Droplet Shape and Solid Concentration on the Suspension Plasma Spraying,”International Journal of Heat and Mass Transfer.,vol. 161, p.120317, November 2020.

[16] N. Zeoli, S. Gu, and S. Kamnis,“RETRACTED: Numerical Modelling of Metal Droplet Cooling and Solidification,”International Journal of Heat and Mass Transfer., vol. 51, no. (15-16), pp. 4121-4131, July. 2008.

[17] P.S. Grant, B. Cantor, and L. Katgerman,“Modelling of Droplet Dynamic and Thermal Histories during Spray Forming-II. Effect of Process Parameters,”Acta Metallurgica et Materialia., vol. 41, no. 11, pp. 3109-3118, November. 1993.

[18] S. Alavi, and M. Passandideh-Fard,“The Effects of Thermal Shrinkage on Coating Formation in Thermal Spray Processes: A Numerical Approach,”18th Annual International Conference on Mechanical Engineering-ISME2010.,Sharif University of Technology, Tehran, Sharif University of Technology, Iran, 11-13 May. 2010.

[19] J.F. Sánchez-Pérez, G. Jorde-Cerezo, A. Fernández-Roiz, and J.A Moreno-Nicolás,“Mathematical Modeling and Analysis Using Nondimensionalization Technique of the Solidification of a Splat of Variable Section,”Mathematics., vol. 11, no. 14, p. 3174, July. 2023.

[20] J. Xie, D. Nélias, H. Walter-Le Berre, K. Ogawa, and Y. Ichikawa,“Simulation of the Cold Spray Particle Deposition Process,”Journal of Tribology.,vol. 137, no. 4, p. 041101, October. 2015.

[21] M. Xue, Y. Heichal, S. Chandra, and J. Mostaghimi,“Modeling the Impact of a Molten Metal Droplet on a Solid Surface Using Variable Interfacial Thermal Contact Resistance,” Journal of Materials Science., vol. 42, no. 1, pp. 9-18, January. 2007.

[22] Y.M. Liao, Y.Z. Zheng, Z.H. Zheng, and Q. Li,“Numerical Simulation of Zirconia Splat Formation and Cooling during Plasma Spray Deposition,”Applied Physics A.,vol. 122, no. 7, p. 654, June. 2016.

[23] S. Li, W. Zhengying, D. Jun, W. Pei, and L. Bingheng, “A Numerical Analysis on the Metal Droplets Impacting and Spreading out on the Substrate,”Rare Metal Materials andEngineering., vol. 46, no. 4, pp. 893-98, April. 2017.

[24] S. Danouni, A. Abdellah El-hadj, M. Zirari, and M. Belharizi,“A Thermo-Mechanical Analysis of a Particle Impact during Thermal Spraying,”Applied Surface Science.,vol. 371, pp. 213-23, May. 2016.

[25] Y. Zhao, Z. Yu, M.P. Planche, A. Lasalle, A. Allimant, G. Montavon, and H. Liao,“Influence of Substrate Properties on the Formation of Suspension Plasma Sprayed Coatings,” Journal of Thermal Spray Technology., vol. 27, no. 1-2, pp. 73-83, January. 2018.

[26] C. Premaram, P.U. Gaur, A.P. Mobarsa, and K. Chaudhary,“Thermal Spray Coating Applications in Tribology: Recent Case Studies,”Journal of Thermal Spray and Engineering., vol. 4, pp. 87-93, January. 2024.

[27] Z. Tang, T. Yang, C. Zhang, W. Wang, S. Liu, W. Liu, and C. Liu,“Influence of Spray Angle on Particle Deposition and Thermal Shock Lifetime of Embedded Micro-Agglomerated Particle Coatings,”Journal of Coatings., vol. 14, no. 199, pp. 1-19, February. 2024.

[28] M. Zirari, A. Abdellah El-Hadj, and N. Bacha,“Numerical analysis of partially molten splat during thermal spray process using the finite element method,”Journal of Applied Surface Science.,vol. 256, no.11, pp. 3581-35-85, Mach. 2010.

[29] M. Pasandideh-Fard, and J. Mostaghimi,“On the Spreading and Solidification of Molten Particles in a Plasma Spray Process Effect of Thermal Contact Resistance,”Plasma Chemistry' and Plasma Processing., vol. 16, pp. S83-S98, March. 1995.

[30] S. Oukach, H. Hamdi, M. El-Ganaoui, and B. Pateyron,“Thermal Effects on the Spreading and Solidification of a Micrometric Molten Particle Impacting onto a Rigid Substrate,”Fluid Dynamics & Materials Processing., vol. 8, no. 2, pp. 173-195, January. 2012.

[31] A.T. Dinsdale, and P.N. Quested,“The Viscosity of Aluminium and Its Alloys-A Review of Data and Models,”Journal of Materials Science.,vol. 39, no. 24, pp. 7221-7228, December. 2004.

[32] T.Satish, M.Ankur, SC.Modi. «High-Performance Molybdenum Coating by Wire-HVOF. Thermal Spray Process».2018; 27:757-768.

[33] SC.Okumus. «Microstructures and mechanical characterization of plasma sprayed Al2O3-TiO2 composite ceramic coating on Mo/cast iron substrates». Materials Letters. 2005; 59:3214- 3220.

[34] VARGEL, Christian. Métallurgie de l’aluminium. In : Techniques de l’Ingénieur, traité « Métaux et alliages non ferreux », réf. M4663. Saint-Denis La Plaine: Techniques de l’Ingénieur, 2010.

[35] SAINFORT, Michel. Diagrammes d’équilibre – Alliages ternaires et multi-constitués. In : Techniques de l’Ingénieur, traité « Données physico-chimiques sur les métaux et alliages », réf. M4105. Saint-Denis La Plaine : Techniques de l’Ingénieur, 2003.

[36] CAILLERIE, Jean-Louis et WILMOTTE, François. Plomb et alliages de plomb. In : Techniques de l’Ingénieur, traité « Étude et propriétés des métaux », réf. M510. Saint-Denis La Plaine : Techniques de l’Ingénieur, 1993. DOI : 10.51257/a-v1-m510

List of Publication and Communication

The research work of this thesis has led to the following publication and communication:

1) International Publication

Fathi Boukhazani, Redha Rebhi, Faouzi Didi, Ebrahim E. Elsayed, Mohamed Kezrane. Numerical Modeling of Phase Change Phenomena During Drop/Wall Interaction in the Context of Thermal Spraying, Edelweiss Applied Science and Technology. Vol. 9, No. 11, 637-660 (2025). https://DOI: 10.55214/2576-8484.v9i11.10942.

2) Conferences

National Conference:

1. **Fathi Boukhazani**, Redha Rebhi, Mohamed Kezrane. Particle Morphology and its Impact on the Thermal Spray: a Computational Approach. In :2024 Nat-Conf SSENAM'7-Engineering Application of Mechanics,29-30 April 2024, ABBES LAGHROUR UNIVERSITY OF KHENCHELA.
2. **Fathi Boukhazani**, Redha Rebhi, Mohamed Kezrane. Analysis of thermal exchange during the flattening of molten metal droplets in thermal spraying. In :2024 Nat-Conf NCEA'1-Energy and its Applications, December 18 2024, University of Medea.

International Conference:

1. **Fathi Boukhazani**, Redha Rebhi, Mohamed Kezrane. Impact of particle-substrate thermal exchange in thermal spray simulation. In 2024 Inter-Conf ICENSOS'3-Engineering Naturel and social sciences, May 16-17 2024, KONYA, TURKEY.
2. **Fathi Boukhazani**, Redha Rebhi, Mohamed Kezrane. Thermal spray simulation of heat exchanges between particles and substrates. In 2024 Inter-Conf ICESIS'2- Scientific and innovative studies, April 18-19 2024, KONYA, TURKEY.
3. **Fathi Boukhazani, Redha Rebhi, Mohamed Kezrane. Study of rapid solidification with consideration of undercooling during the flattening of droplets on a substrate in coating formation. In 2024 Inter-Conf ICENSOS'3- Engineering Naturel and social sciences, May 16-17 2024, KONYA, TURKEY.**
4. Fathi Boukhazani, Redha Rebhi, Mohamed Kezrane. **Thermal analyses of particle substrate interactions in the thermal spray simulation.** In 2024 Inter-Conf

ICENSOS’3- Engineering Naturel and social sciences, May 16-17 2024, KONYA, TURKEY.